INVESTIGATION OF GATE CURRENT IN NEUTRON IRRADIATED
$Al_xGa_{1-x}N$/GaN HETEROGENEOUS FIELD EFFECT TRANSISTORS USING
VOLTAGE AND TEMPERATURE DEPENDENCE

THESIS

Thomas E. Gray, Major, USA

AFIT/GNE/ENP/07-02

DEPARTMENT OF THE AIR FORCE
AIR UNIVERSITY

AIR FORCE INSTITUTE OF TECHNOLOGY

Wright-Patterson Air Force Base, Ohio

AFIT/GNE/ENP/07-02

INVESTIGATION OF GATE CURRENT IN NEUTRON IRRADIATED $Al_XGa_{1-X}N$/GaN HETEROGENEOUS FIELD EFFECT TRANSISTORS USING VOLTAGE AND TEMPERATURE DEPENDENCE

THESIS

Presented to the Faculty

Department of Engineering Physics

Graduate School of Engineering and Management

Air Force Institute of Technology

Air University

Air Education and Training Command

In Partial Fulfillment of the Requirements for the

Degree of Master of Science in Nuclear Engineering
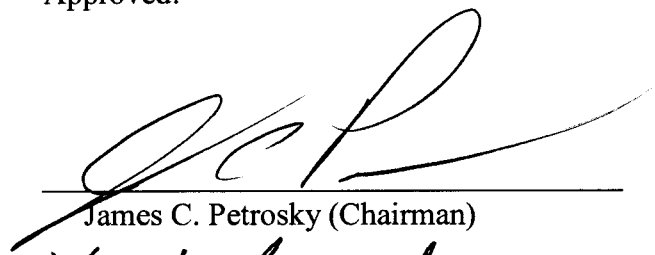
Thomas E. Gray, BA

Major, USA

March 2007

APPROVED FOR PUBLIC RELEASE; DISTRIBUTION UNLIMITED

INVESTIGATION OF GATE CURRENT IN NEUTRON IRRADIATED Al$_x$Ga$_{1-x}$N/GaN HETEROGENEOUS FIELD EFFECT TRANSISTORS USING VOLTAGE AND TEMPERATURE DEPENDENCE
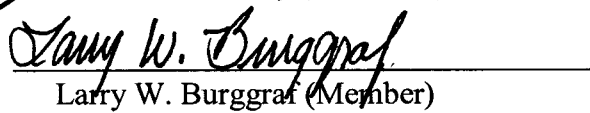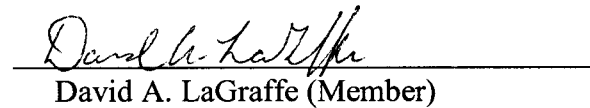
Thomas E. Gray, BA
Major, USA

Approved:

_____
James C. Petrosky (Chairman)

_____
Larry W. Burggraf (Member)

_____
David A. LaGraffe (Member)

_07/Mar 07_____
Date

_7 Mar 2007_____
Date

_7 Mar 07_____
Date

Abstract

The gate current of $Al_{27}Ga_{73}N/GaN$ heterogeneous field effect transistors (HFETs) is investigated using current-voltage (IV) and current-temperature (IT) measurement demonstrating that trap assisted tunneling (TAT) is the primary current mechanism. Excellent fit to experimental data is achieved using a thermionic trap assisted tunneling (TTT) model. A single value for each of the primary parameters (Schottky barrier height, trap energy, donor density and trap density) results in a sigma of 1.38×10^{-8} A for IT data measured at five voltages between 85K and 290K and for IV data measured at three temperatures between 0.0 V and -4.0 V.

High energy (>0.5 MeV) neutron irradiation at fluences between 4.0×10^{10} and 1.2×10^{12} n/cm^2 confirms an increase of gate current with fluence. A change in IV characteristics, interpreted as an increase in magnitude of threshold voltage, is also observed. The TTT model suggests that increased trap density is responsible for increased gate current at a fluence of 1.2×10^{12}. An increase in trap density from the unirradiated fit value of 4.593×10^{21} to 5.737×10^{21} $traps/m^3$ and an increase in the position of traps in the energy band from 0.896 to 0.9028 V results in a fit with σ of 1.77×10^{-9} A. A poorer fit ($\sigma = 4.03 \times 10^{-8}$ A) is achieved by reducing the Schottky barrier height parameter from 1.317 V to 1.238 V suggesting that Schottky barrier height reduction is not responsible for the increase in gate current. Finally, an increase in donor defect density is modeled resulting in a sigma of 5.00×10^{-9} A and an increase in threshold voltage magnitude consistent with the observed change in measured IV behavior.

Acknowledgments

I would like to express my sincere appreciation to my faculty advisor, Dr. James Petrosky, for his guidance and support throughout the course of this thesis effort. His insight and experience were certainly appreciated. The financial support of the Air Force Office of Scientific Research provided the funding for this work. I would also like to thank the very capable staff at the Ohio State University Research Reactor.

I especially wish to thank my father, a farmer and machinist who encouraged my curiosity as a child, taught me discipline and the beauty of precision, and continues to challenge me to think critically.

Thomas E. Gray

Table of Contents

List of Figures

List of Tables

INVESTIGATION OF GATE CURRENT IN NEUTRON IRRADIATED

$Al_xGa_{1-x}N$/GaN HETEROGENEOUS FIELD EFFECT TRANSISTORS USING

VOLTAGE AND TEMPERATURE DEPENDENCE

I. Introduction

Heterogeneous field effect transistors (HFETs) built from aluminum gallium nitride and gallium nitride show great promise as high speed, high power transistors. However, these devices show an undesirably high gate current which is further increased by irradiation. In this thesis theory, modeling and experiment are used to determine the mechanism responsible for this gate current in the as-manufactured state and the reason for the increase in gate current after irradiation. The following sections will cover the importance of these devices to military and civilian systems, the physics behind their operation, and the objectives and methods used in this thesis effort.

Background

GaN technology has seen increased use over the last fifteen years and, although still much more expensive to manufacture than silicon and gallium arsenide, the cost to manufacture has decreased as more reliable methods have been found to grow the GaN lattice and improve lattice quality.

The materials most commonly used in the production of semiconductors, silicon and gallium arsenide (GaAs) among others, have physical characteristics that make them poorly suited for high power, high frequency applications or optics applications that involve ultraviolet wavelengths [1]. Gallium nitride (GaN) based materials have

characteristics which make them much better suited for these applications. Devices such as visible and ultraviolet light emitting diodes and lasers have been developed and marketed based on GaN [1,2]. The wide bandgap of GaN (3.49 eV) and AlGaN (3.80 eV for 0.27 Al molar concentration) devices enable them to emit and absorb photons in the near ultraviolet spectrum whereas the narrower bandgap of silicon based devices (1.12 eV) and GaAs devices (1.43 eV) limits their usefulness to the infrared. The wider bandgap of GaN devices also enables them to operate at higher temperatures than silicon and GaAs devices without a change in performance due to the elevation of electrons from the valence band to the conduction band by thermal energy (phonons). Furthermore, GaN has a higher thermal conductivity (up to 1.97 W/cm-K depending on lattice dislocation density) than silicon (1.30 to 1.45 W/cm-K) or GaAs (0.55 W/cm-K) which enables heat to be more rapidly removed to the device substrate.

The Defense Advanced Research Projects Agency (DARPA) and the Office of Naval Research (ONR) have funded major research programs to develop GaN for use in military systems. The high speed and high power capabilities of GaN make it well suited for military radar applications. A GaN based high power microwave device has been demonstrated which produced 30.6 W/mm of gate width at an operating frequency of 8 GHz [3]. In contrast, GaAs based devices have a limit of operation of 1 W/mm at 10 GHz [4] and are more susceptible to damage by radiation. Silicon based devices are even more limited.

GaN devices have been shown to be more tolerant of radiation damage than Si and GaAs based devices. GaN devices operate without significant degradation at a high

energy (300-1400 keV) electron fluence that is 2 to 3 orders of magnitude higher than for

the equivalent GaAs device [21]. This may be due to fact that Ga-N bonds are stronger

than the Ga-As bonds. Stronger bonds resist displacement and reduce the number of

defects created by radiation. For example, it has been shown that GaN samples irradiated

by 1.0 MeV electrons at a fluence of $1x10^{17}$ e/cm^2 undergo a reduction of 50% in

cathodoluminescence because of reduced carrier density. GaAs material tested under the

same conditions undergoes a carrier removal rate that is 2 times higher than GaN and that

the luminescence intensity degrades to less than 1% of the original value [5]. Because of

its inherent radiation hardness, an important proposed use for GaN devices is in satellite

based radar systems, which operate at low temperatures and are subject to damage by the

near earth orbit radiation environment.

This brings us to the intent of this proposed work, which is to discover the cause

of gate current in as-grown AlGaN/GaN HFETs and the mechanism responsible for the

increase in gate current after neutron irradiation.

Gallium Nitride Device Physics

The device under study is an HFET based on an AlGaN/GaN heterostructure.

The architecture of the device is shown in Figure 1. The AlGaN layer grown on top of the

GaN layer comprises the heterojunction. Current flows from the drain to the source

through a highly conductive 2 degree electron gas (2DEG) that is created at the

heterojunction. The transistor action of the device is controlled by the voltage on the

gate, which acts to increase or decrease the density, and therefore the conductivity, of the

2DEG. The gate contact is a Schottky barrier created by the difference in electron

3

affinity between the gate metal and the AlGaN. This difference in electron affinity results in a large (> 1eV) potential barrier. The source and drain are ohmic contacts and do not have a significant barrier.

The 2DEG is spontaneously created at the heterojunction as a result of the GaN and AlGaN crystal structures. GaN is a III-V material which forms a Wurtzite crystal structure in which the electrons are not shared equally in the covalent bonds resulting in a spontaneous polarization in the crystal. By replacing a fraction of the gallium atoms with aluminum atoms, AlGaN is created, which also has a spontaneous polarization. The heterojunction is created by growing a thin later of AlGaN on a base of GaN. Because the AlGaN lattice constant is slightly smaller than the GaN lattice constant the AlGaN crystal stretches to match bonds with the GaN. This changes the charge distribution in the AlGaN and gives rise to a piezoelectric polarization which points in the same direction as the spontaneous polarization. The change in polarization between the AlGaN (spontaneous plus piezoelectric) and the GaN (spontaneous) at the heterojunction results in a layer of net positive charge. The electric field created by this positive charge draws conduction electrons from the AlGaN and the GaN and forms the 2DEG.

The positive charge layer at the heterojunction is sometimes called a conduction band discontinuity. This discontinuity results in a quantum well as shown in Figure 1. This quantum well is on the order of an electron deBroglie wavelength wide. Electrons trapped in the well form a standing wave and move easily in the plane of the interface.

For the HFETs under study, the 2DEG concentration is typically on the order of 10^{13} electrons/cm^2 and is 2 nm thick. The 2DEG concentration depends on several

4

factors. One factor is the Al concentration in the AlGaN layer, which determines the

magnitude of polarization at the AlGaN/GaN interface. The 2DEG concentration is also

determined by the applied gate voltage which acts to change the depth of the quantum

well. Applying a negative gate voltage (V_g) with respect to the drain and source ohmic

contacts raises the energy of the bottom of the quantum well with respect to the Fermi

level of the electrons. This reduces the concentration of electrons in the 2DEG.

Applying a sufficiently large negative gate voltage raises the quantum well above the

Fermi level and eliminates the 2DEG, turning off the device. V_{th} is defined as the value

of V_g at which the 2DEG becomes too small to carry significant current. This can be

done very rapidly and accounts for the excellent high speed performance of AlGaN/GaN

HFETs.
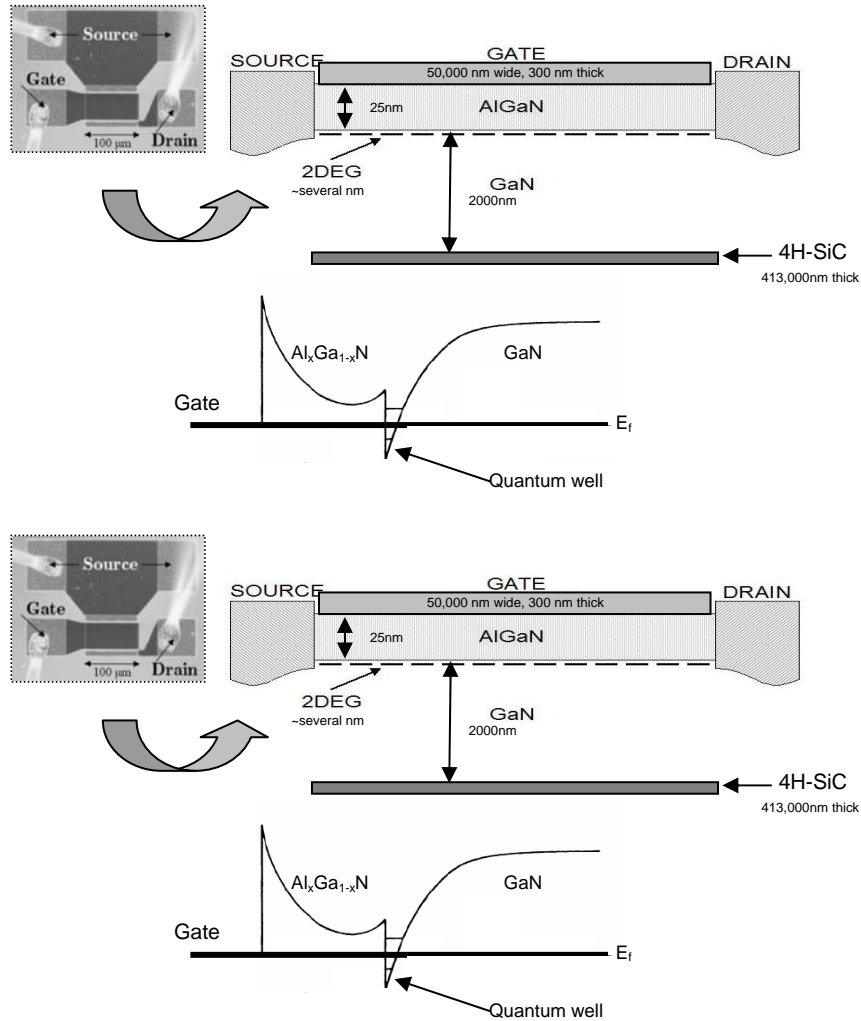
Figure 1. AlGaN/GaN HFET physical structure and band diagram[8].

Predictable effective gate voltage is essential to the reliable operation of the HFET. In an ideal HFET the gate current is always zero. In a real HFET gate currents are on the order of hundreds of microamps per mm of gate width [6,7]. The drop in voltage as the current moves through the gate and resistive AlGaN layer changes the effective gate voltage. This results in an undesired change in source to drain current and higher power requirements.

The gate current in the HFET devices under study has been observed to increase with neutron irradiation [6,7]. The primary effect of neutron irradiation is to create lattice defects. Several mechanisms have been proposed [7,8,9,13,16,17] to explain the change in gate current after irradiation. These will be discussed in the literature review section.

The focus of this research is to discover the dominant mechanism for gate leakage in AlGaN/GaN HFETs and to use the model describing that mechanism to determine the cause of increased gate leakage after neutron irradiation.

Research Justification

The mechanism responsible for the gate current in irradiated AlGaN/GaN HFETs has not been determined [6,7,8]. Determining the mechanism responsible will enable engineers to design HFETs without large gate currents. Furthermore, determining the mechanism responsible for increased gate current after irradiation is necessary so that increased gate current can be prevented, enabling the use of AlGaN/GaN technology in harsh radiation environments such as satellites or nuclear reactors.

Problem Statement

What is the mechanism responsible for gate current in AlGaN/GaN HFETs? Can analysis of the voltage and temperature dependence of the gate current determine the mechanism responsible for producing gate current? What is the cause of increased gate current after neutron irradiation?

Hypotheses

It can be demonstrated using voltage dependent gate current measurement (IV) and temperature dependent gate current measurement (IT) that the gate current is

consistent with trap assisted tunneling mechanism and is not consistent with other

mechanisms (generation recombination, direct tunneling, field emission, surface leakage).

Trap assisted tunneling through the gate Schottky barrier is the dominant gate current

leakage mechanism for AlGaN/GaN HFETs.

Neutron irradiation will increase the gate current. Analysis of the change in gate

current using a trap assisted tunneling model will reveal the mechanism responsible.

Research Objectives

1. Determine the dominant current mechanism for neutron irradiated AlGaN/GaN

HFETs.

2. Design, construct and test an experimental apparatus that enables neutron

irradiation at liquid nitrogen temperatures over a period of hours in order to prevent

neutron induced defects from annealing prior to current measurement.

3. Irradiate HFETs with neutrons to increase the trap density through knock-on

damage and measure the change, if any, in gate current.

4. Use IV and IT measurement and modeling to determine the cause of increased

gate current.

Scope

This research is limited to the determination of the dominant current producing

mechanism in heterogeneous junction $Al_{27}Ga_{73}N/GaN$ HFETs at gate voltages between

0.0 and -8.0V and temperatures between 77 and 300K. Increased gate current after

irradiation with >0.5 MeV neutrons is studied at fluences between 4.0×10^{10} and 1.2×10^{12}

n/cm^2.

Methodology

Theoretical development, modeling, and experimental measurements were used in this effort. Current transport models for metal-semiconductor contacts were used in the development of the gate current model [10,11]. Trap assisted tunneling through the gate Schottky barrier was modeled as a statistical process [12, 15, 16]. The expected contribution of each transport process to the overall gate current model was determined using accepted physical constants, nominal values for gate dimensions, and order-of-magnitude values for physical parameters of the devices which are not known with precision, such as doping and trap density. The sensitivity of the gate current models to bias voltage, temperature, Schottky barrier height, and other variables was determined by direct calculation. The gate currents before and after irradiation were measured as a function of gate voltage and device temperature and the results were compared with the models. Model parameters were then varied to find the best fit to IV and IT data and to suggest causes of increased current after irradiation.

Assumptions/Limitations

It is assumed that the mechanism primarily responsible for the gate current dominates other proposed mechanisms and that the primary mechanism will have IV and IT behaviors characteristic to the primary mechanism alone.

It is assumed that the gamma irradiation that occurs during neutron irradiation will not contribute significantly to the creation of defects because of the low non-ionizing energy loss of gamma rays in AlGaN and GaN.

Sequence of Presentation

   This thesis is separated into six chapters. This first chapter has provided background information on the research effort. Chapter 2 presents the results of the literature search and details the HFET gate leakage models. Chapter 3 presents the modeling and design of the experimental apparatus. Chapter 4 describes the experimental setup and the experimental procedure before, during and after irradiation. The results of the experiments are presented in chapter 5. Finally in chapter 6, conclusions and recommendations for future studies are given.

II. Research Review and Model Development

Chapter Overview

A review of recent AlGaN/GaN HFET research identified three gate leakage

models (by Svensson, et. al., Karmalkar and Sathaiya, and Hashizume et. al.) in addition

to well established Schottky barrier charged particle transport models (field emission,

etc.). Possible leakage paths from the HFET gate to source/drain are considered and a set

of plausible leakage models are selected for further study. The plausible models

(thermionic emission, thermionic field emission, Svensson trap assisted tunneling

(STAT), and thermionic trap assisted tunneling (TTT)) are developed and analyzed for

sensitivity to changes in their primary parameters. Finally, a MATLAB based fitting

routine is developed to aid in analysis of measured IV and IT data.

Gate Current Models

Several models have been proposed to explain gate leakage in AlGaN/GaN

devices. These include the well understood mechanisms of field emission, thermionic

emission, surface leakage, and generation-recombination. These will be considered in the

model development section of this chapter, as will a leakage model developed by

Svensson et. al. to describe trap assisted tunneling through a Schottky barrier at an

interface consisting of $Si/SiO_2/Si_3N_4$ [12]. Two models specifically developed to

investigate gate leakage in AlGaN/GaN devices will be considered in this section. The

first was developed by Karmalkar and Sathaiya of the Indian Institute of Technology

[15,16] and assumes trap assisted tunneling through the Schottky barrier. The second

model, developed by Hashizume, et. al. of Hokkaido University [17], assumes thermionic

emission through a Schottky barrier which has been made thinner by the presence of surface defect donors.

Karmalkar and Sathaiya argue that the reverse bias gate current in AlGaN/GaN HFET devices is due to two parallel gate to substrate tunneling paths. The first path is due to direct tunneling (field emission) across the gate Schottky barrier, and the second path is due to tunneling through the Schottky barrier via deep traps distributed throughout the AlGaN layer and spread over an energy band located within the Schottky barrier height [15,16]. The direct tunneling path makes a negligible contribution to the current at temperatures above 500K because of the width of the Schottky barrier. The trap assisted tunneling path dominates transport through the Schottky barrier at temperatures below 500K.

Karmalker and Sathaiya developed a model to calculate the reverse bias gate current based on trap assisted tunneling and found that the model gave good fit to experimental data. This model assumes a continuum of trap energies within the band gap of the AlGaN. Figure 2 shows the HFET structure and biasing arrangement used by Sathaiya (a) and modeled energy band diagram from gate to substrate (b). The energy band diagram shows both the direct tunneling (DT) and the trap assisted tunneling (TT) processes. The traps are spread over an energy band ($\phi_2 \leq \phi \leq \phi_1$) within the barrier height. The AlGaN/GaN conduction band discontinuity ($\Delta\phi_c$), gate Schottky barrier height (ϕ_B) and potential due to gate voltage (ϕ_F) are shown. Also shown is the distribution of trap concentration N_t over energy.
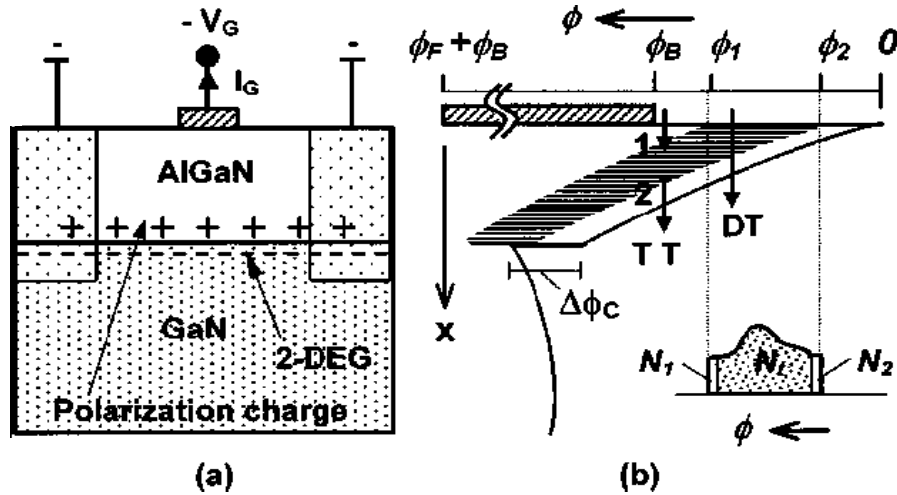
Figure 2. (a) Sathaiya AlGaN HFET device structure, (b) band diagram [15].

Karmalkar and Sathaiya applied this model to HFETs which had a high density of traps. They found that the gate current was high (10^{-4} A) and almost insensitive to temperature between 100 and 300 K. After plasma treatment, which reduced the density of traps by a factor of ~100, the gate current was reduced to 10^{-9} A at 300 K and showed a large dependence on temperature. The gate current was observed to increase by a factor of ~30 from 100 to 300K. They attribute the decreased gate current to a reduction in the density of traps. They attribute the increased dependence on temperature to a decrease in the energy level of the lower limit of the trap energy band (ϕ_1). A decrease in the parameter ϕ_1 reduces the width of the trap energy band and reduces the energies at which trap assisted tunneling can occur. Reducing the width of the energy band trap also contributes to increased temperature dependence. It is important to note that ϕ_1, the density of traps, and the energy level of the upper limit of the trap band (ϕ_2) are fitting parameters which were adjusted to make the model fit the observed IV and IT

13

measurements. Sathaiya did not report that these values were confirmed by any other measurement technique.

A simplified model for trap assisted tunneling, which assumes a single trap energy within the AlGaN band gap, has recently been developed by Karmalkar and Sathaiya [16]. This simplified model also provides an excellent fit to empirical data. This model will be discussed in the modeling section of this chapter and used to analyze the gate current of HFETs in this effort.

Another gate leakage mechanism is proposed by Hashizume, et. al. [17]. They proposed Schottky barrier thinning as the cause of leakage current in as grown GaN and AlGaN Schottky diodes. Their model was based on thermionic field emission and included the effects of barrier thinning caused by unintentional surface-defect donors. The donors are assumed to be deep donors with a high density near the surface of the semiconductor which decays exponentially with depth (Figure 3). A nitrogen vacancy is identified as the deep donor. The positive space charge created by the donors bends the conduction band and makes the Schottky barrier thinner. The thin Schottky barrier enhances thermionic field emission tunneling. Thee model was used to fit IV and IT measurements taken from AlGaN diodes achieving good fitting results at forward and reverse biases and varying temperatures.
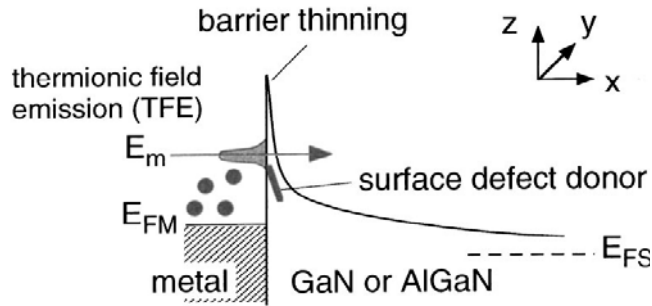
Figure 3. Thin surface barrier model [15].

Although Hashizume's results appear very promising, as shown in Figure 4, there
was insufficient detail in the paper to permit further investigation in this thesis effort.
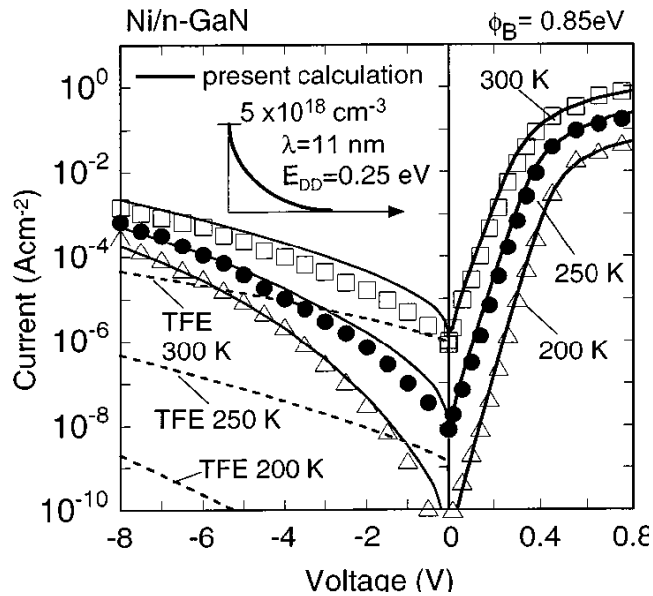
**Figure 4. I-V-T characteristics of the Ni/n-GaN diode. The solid and the broken
lines represent the calculated results by Hashizume's method and unmodified TFE
model, respectively [15].**

Irradiation Damage

GaN device response to radiation damage has not been as thoroughly researched
as radiation damage in silicon and gallium arsenide. Most GaN radiation damage

research that has been conducted has focused on proton damage [9,13,14]. Some work, notably at the Air Force Institute of Technology, has investigated the effects of high energy electrons and neutrons [5,6,7,8]. These research efforts have resulted in conflicting conclusions as to the cause of increased gate current after irradiation.

White, et. al. [9,13] used cathodoluminescent spectroscopy to study the effects of 1.8 MeV protons on AlGaN/GaN HFETs and diodes as part of a multi university research initiative (MURI) for Radiation Physics supported by Air Force Office of Scientific Research under MURI grant F49620-99-1-0289. Low energy, electron-excited nanoscale-luminescence enabled measurement of the change in electrical characteristics due to proton fluence at varying depths in the semiconductor. They observed that the effective donor doping concentration, magnitude of the threshold voltage and Schottky barrier height reduced with increasing proton fluence. The reduction in effective donor doping was attributed to an increased concentration of either Ga vacancies or complexes. The Ga vacancies are deep acceptor defects which would compensate the existing donors. The observed lowering of the Fermi level is consistent with an increased concentration of acceptors. The decrease in magnitude of the threshold voltage (Figure 5) can also be explained by the lowered Fermi level. The lowered Fermi level would reduce the amount by which the conduction band discontinuity between the AlGaN and GaN would be below the Fermi level. Therefore a less negative threshold voltage would be sufficient to raise the conduction band discontinuity above the Fermi level and eliminate the 2DEG. The reduction in magnitude of threshold voltage due to removal of carriers by acceptor

16

defects, and resulting decrease in 2DEG carrier density and lowering of Fermi level, was

also observed by Hu et. al. [14].
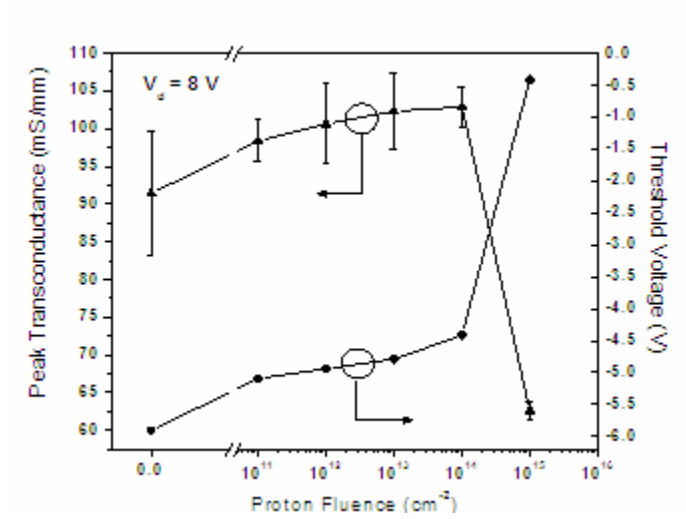
Figure 5. Effect of 1.8 MeV proton fluence on AlGaN/GaN HFET [13].

The change in material properties responsible for the reduction in Schottky barrier

height, shown in Figure 6, was not explained in the AFOSR Radiation Physics MURI.
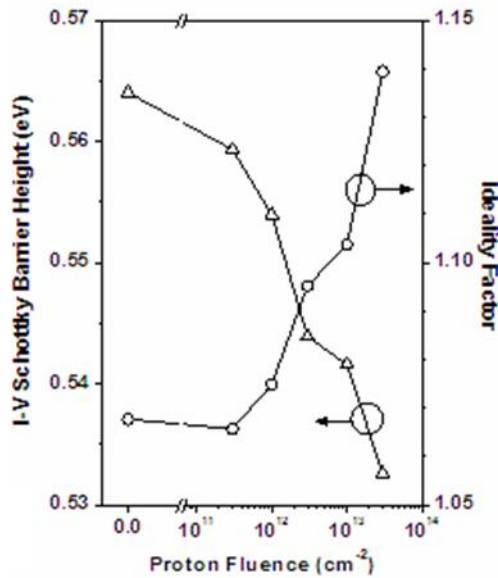
Figure 6. Schottky barrier height reduction with fluence [13].

The effect of irradiation on gate leakage was not reported in the MURI results, but it is reasonable to assume that the gate current would increase with the observed lowering of the Schottky barrier height. Therefore a lowered barrier height will be considered as a potential cause for increased gate leakage current after irradiation.

Previous work at the Air Force Institute of Technology has investigated the effects of high energy electrons and neutrons on the function of GaN devices [5,6,7,8,20]. Uhlman [8] conducted low temperature IV measurements of the gate current and concluded that trap assisted tunneling (TAT) is the primary current mechanism.   He observed a substantial radiation-induced increase in gate current. Uhlman hypothesized that the increase in gate current was due to an increase in trap assisted tunneling resulting from a radiation induced increase in the density of traps at the metal-semiconductor junction. Roley [7] attempted to determine the cause of increased gate current using

temperature dependence but because of problems with his experimental apparatus was unable to gather sufficient data. He did demonstrate that the voltage dependence of the gate current was consistent with TAT, but his results were not conclusive.

Uhlman and Roley used a model based on Svensson's work [12] (called the STAT model in this thesis). The STAT model and the simplified single trap energy trap assisted tunneling model developed by Sathaiya [15] (the thermionic trap assisted tunneling model, TTT) are discussed in the next section.

Model Development

In this section the architecture of the HFET is considered and possible current paths are proposed. The expected contribution of each gate current leakage model to the gate current is considered and some current paths and leakage models are eliminated as candidates. The remaining models are then further developed in order to support the experimental effort described in the next chapter.

Gate current in a HFET can be modeled as shown in Figure 7. Three possible current paths are proposed: along the surface of the AlGaN from gate to source (1); through the AlGaN (2); through the AlGaN and along the 2DEG (3). The source and drain are interchangeable in the HFET, so these current paths also apply to gate-to-drain current.
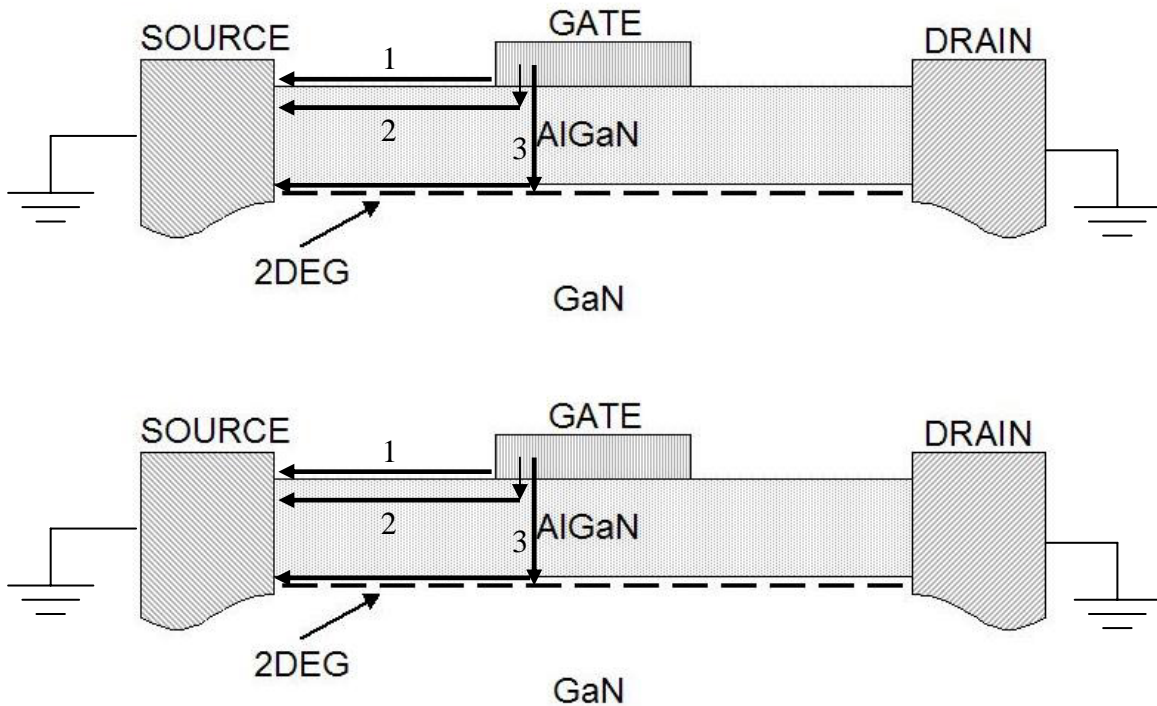
Figure 7. Proposed current paths.

Electrons may move along each of the paths depicted in the Thevenin equivalent circuit in Figure 8. This Thevenin equivalent circuit represents each charged particle transport mechanism as an equivalent resistance. The equivalent resistance for each mechanism would be inversely proportional to the probability of transport of an electron by that mechanism. Where the equivalent resistances are in parallel, the mechanism with the lowest resistance will dominate the current. For instance, if FE provides the lowest resistance current path through the Schottky barrier then FE will dominate the current through the barrier. Where the equivalent resistances are in series, the greatest resistance dominates the current. The physical mechanisms supporting current along each path are discussed below.
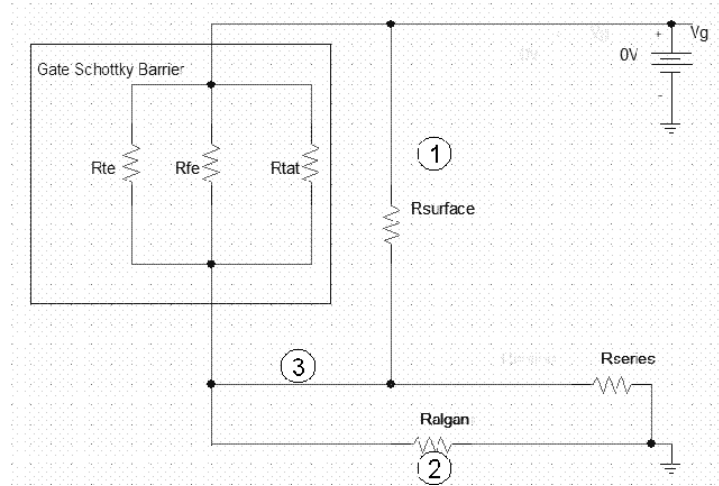
Figure 8. Thevenin equivalent circuit based on proposed current paths.

For path (1) the current results from surface leakage, which could be caused by a thin film of conductive residue at the surface or by defect hopping. Defect hopping is plausible because there is expected to be a high density of defects at the surface because of broken bonds. These broken bonds are due to the absence of atoms to contribute to covalent bonding at the surface.

It is assumed that surface leakage current is a function of electric field, which increases with gate voltage. The voltage drop between the gate and source continues to increase with increasing $|V_g|$ even beyond V_{th}. The gate current (I_g) has been demonstrated to saturate for gate voltage beyond the threshold voltage [14]. This indicates that surface leakage is not the dominant mechanism contributing to I_g. Therefore path (1) is not the dominant current path.

Paths (2) and (3) require the transport of electrons across the Schottky barrier at the gate/AlGaN interface. In the absence of in-band traps, transport across Schottky

barrierers takes place by a combination of thermionic emission (TE), thermionic field emission (TFE), field emission (FE), and generation recombination (GR). Electrons would move from the left (gate) to the right (AlGaN) in Figure 9.

(a) Thermionic emission   (b) Thermionic-field emission   (c) Field emission.
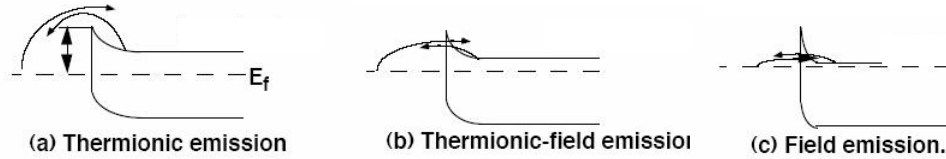
Figure 9. Band model of Schottky barrier current transport (TE, TFE, FE).

Conduction band electrons with sufficient kinetic energy are transported over the barrier under the influence of the electric field in TE. The kinetic energy required for TE is provided by thermal energy. The average kinetic energy of electrons at low temperatures (~.01 eV at 77K) is much less than the Schottky barrier height at the gate. The Schottky barrier height (ϕ_b) at the gate interface for AlGaN/GaN devices can be calculated using an empirical formula [18]

$$\phi_b = 0.7841 + 1.8559(x_{Al}) \text{ eV,}$$

where x_{Al} is the molar concentration of Al in the AlGaN. With $x_{Al} = .27$ for the HFETs under study, ϕ_b is calculated as approximately 1.3 eV.

The presence of higher energy electrons at the upper end of the Gaussian distribution of thermal energy and proposed lowering of barrier height [13] makes TE a possible contributor to I_g.

TFE and FE occur by direct tunneling through the Schottky barrier. In most FE models the barrier is assumed to be triangular. This results in a dependence of I_g on temperature because at higher temperatures the electrons will be at higher energies when they encounter the barrier and will 'see' a smaller barrier width which increases the probability of tunneling. The model for TFE includes FE as the lowest electron kinetic energy case, in which the electron tunnels through the base of the barrier. TFE (including FE) is a possible contributor to I_g.

Another mechanism, generation-recombination (GR), is due to an electron being elevated from the valence band to the conduction band in the barrier region. The energy required to elevate the electron to the conduction band could be provided by thermal energy or photons. The electric field in the barrier region would then carry the electron through the barrier region into the AlGaN. Because the barrier region is in the AlGaN, and the band gap between the conduction band and the valence band is large in AlGaN (~3.8 eV) [5], the probability of elevation of an electron from the conduction band by thermal energy is vanishingly small in the temperature range of interest. Therefore GR is not a viable mechanism for producing I_g.

The final mechanism proposed to enable transport through the Schottky barrier is trap assisted tunneling (TAT). TAT requires the presence of traps in the band gap of the semiconductor. The TAT model also predicts that the gate current will have a small temperature dependence compared to the almost exponential dependence predicted by the TE and TFE models. TAT, TE and TFE will be investigated as contributors to gate current.

Once through the Schottky barrier, path (2) assumes the drift of electrons through the AlGaN parallel to the gate. This is extremely unlikely because the electric field is perpendicular to the gate. Therefore path (2) is not a viable current path. Eliminating path (2) simplifies the Thevenin equivalent circuit as shown in Figure 10.
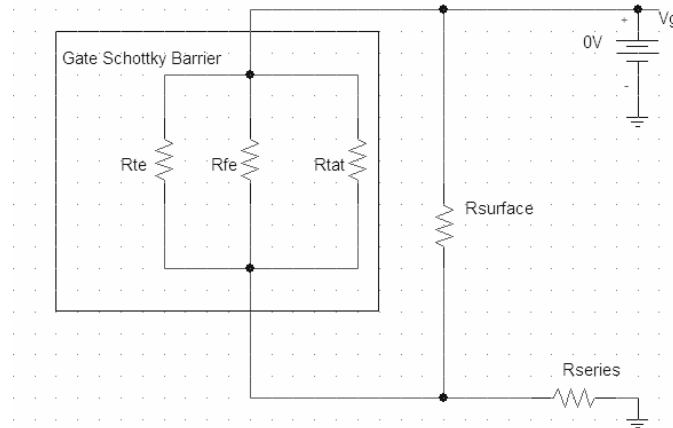
Figure 10. Simplified Thevenin equivalent circuit.

Path (3) requires the transport of electrons across the Schottky barrier, drift of electrons through the AlGaN into the 2DEG under the influence of the electric field, and diffusion along the 2DEG to the source contact. Transport across the Schottky barrier has already been described. Drift through the AlGaN and along the 2DEG is determined by the electric field and the resistivity of the AlGaN and 2DEG, respectively.

TE, TFE and TAT (described by both the STAT and the TTT models), are proposed as mechanisms for gate current. Each of these models has a 'signature' dependence on gate voltage and temperature, which will now be demonstrated.

Thermionic Emission. The expression describing TE current in forward bias for a Schottky diode is Equation 2 [10]

$$I_{TE} = I_0 e^{\frac{-qV_G}{kT}} \tag{1}$$

with

$$I_0 = AA^*T^2 e^{\frac{-q(\phi_B - \Delta\phi)}{kT}}$$

and

$A =$ area of device

$A^* =$ effective Richardson constant

$q =$ magnitude of electronic charge

$k =$ Boltzmann's constant

$V_G =$ bias on the gate relative to the source.

In negative bias $I_{TE} = -I_0$ and is nearly constant with voltage until the electric field produced by V_g is large enough to produce avalanche breakdown. Avalanche breakdown in AlGaN happens at electric fields greater than $2.5\text{x}10^6$ V/cm [5]. V_{th} for the HFETs under study is approximately 4V and the width of the AlGaN is 25nm. This gives a maximum electric field of $1.6\text{x}10^6$ V/cm. Because the HFET is not operated at a large enough V_g to produce avalanche breakdown, I_{TE} will be taken as constant in reverse bias.

Using the constants given in the Appendix for these devices and Equation 1, current due to TE is expected to be on the order of 10^{-15} A at room temperature and have a high dependence on temperature, as shown in Figure 11.
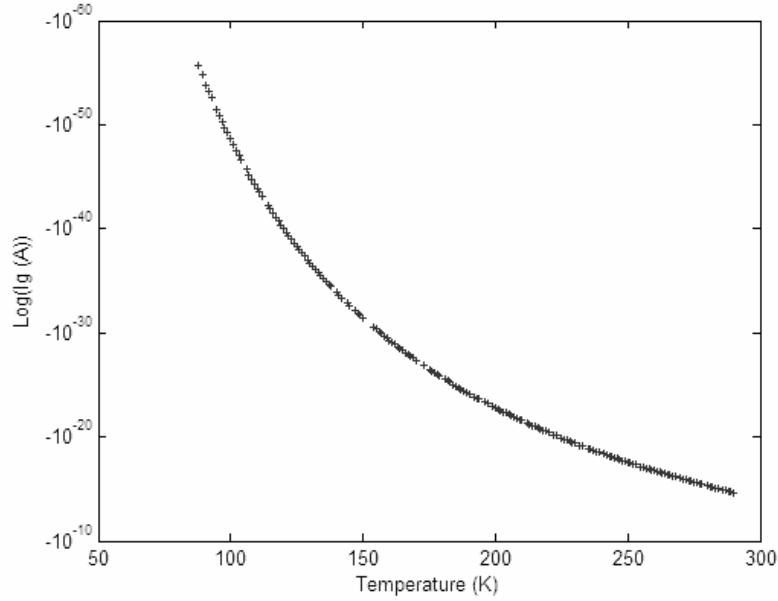
Figure 11. Dependence of TE on temperature (Vg = -4.0 V).

Thermionic Field Emission. The expression describing TFE is given for highly doped ($\sim10^{17}$ donors/cm^3) Schottky junctions in Equation 3 [10]. The as-grown donor density for GaN, due to defects, is on the order of 10^{18} donors/cm^3. The density in AlGaN is assumed to be similar.

$$I_{TFE} = I_{FE0} \left(e^{\frac{qV}{E_0}} - 1 \right)$$
(2)

with

$$I_{FE0} = \frac{AA^* T \sqrt{(\pi q E_{00}(\phi_b - V))}}{k \cosh \frac{E_{00}}{kT}} e^{\left(-\frac{q\phi_b}{E_0}\right)}$$

and

$$E_0 = E_{00} \cot\left(\frac{E_{00}}{kT}\right)$$

$$E_{00} = \frac{qh}{2} \sqrt{\frac{N_d}{\varepsilon_s m^*}} \ .$$

As with TE, current due to FE is expected to be small ($\sim 10^{-20}$ A) at room

temperature and be highly dependent on temperature (Figure 12).
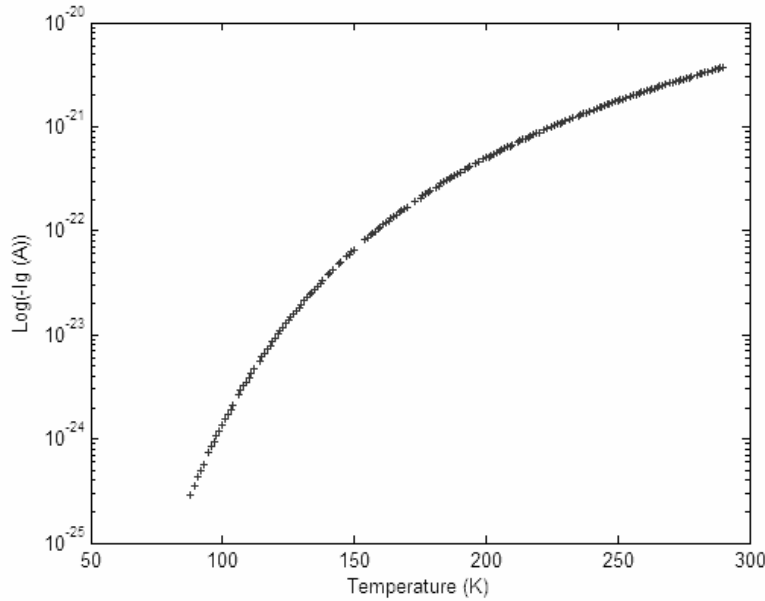
Figure 12. Dependence of FE on temperature (Vg = -4.0V).

Trap Assisted Tunneling. Two separate models of trap assisted tunneling (TAT)

are considered. The first was developed by Svensson, et. al. [12] and will be referred to

as the STAT model. The STAT model was used by Uhlman and Roley in previous work

27

on AlGaN/GaN HFETs. The STAT model assumes thermally excited electrons tunneling via traps distributed homogeneously throughout the AlGaN. The STAT current is calculated by spatial integration. The second model considered was recently developed by Sathaiya and Karmalkar [15,16] and is referred to as the thermionic trap assisted tunneling (TTT) model. TTT also assumes thermally excited electrons and a homogeneous trap distribution. The TTT current is calculated by integration over easily determined energy limits compared to the spatial limits of the STAT model, which are difficult to determine. A brief derivation of each model will now be presented in order to compare the models.

The Svensson derivation is for MNOS devices and describes the transport of electrons under the influence of an electric field from a Si layer through a SiO_2 layer to a Si_3N_4 layer. The theory does not assume any material specific properties and can be applied generally. Here the model will be applied to the Schottky barrier at the metal/AlGaN interface of the HFET. In this case the SiO_2 layer in the Svensson derivation corresponds to the metal gate layer in the HFET and the Si_3N_4 corresponds to the AlGaN. The presence of the SiO_2 term in the Svensson theory does not fit the HFET architecture and so the SiO_2 term will be eliminated. A derivation of the STAT model tailored for HFET devices is presented here.

The band diagram used for this derivation is shown in Figure 13. The value of V_g is taken as V_{th}.
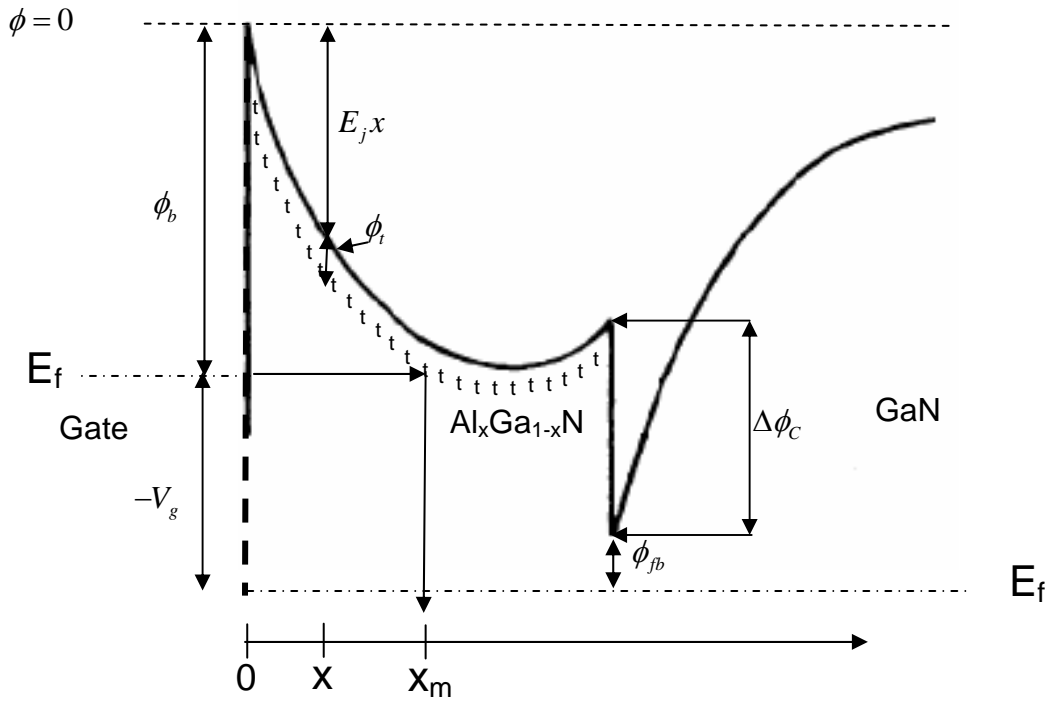
Figure 13. Trap assisted tunneling (TAT) band model.

This model assumes a uniform trap density throughout the AlGaN layer at a single potential ϕ_t below the AlGaN conduction band. ϕ_{fb} is equal to the amount of energy by which the bottom of the conduction band discontinuity $\Delta\phi_c$ is above the Fermi energy.

The rate of change of electron concentration in the traps is described by

$$\frac{\partial n_t}{\partial t} = \frac{(N_t - n_t) f_{metal}}{\tau_1} - \frac{n_t (1 - f_{AlGaN})}{\tau_2} \qquad (3)$$

with

n_t = concentration of electrons in traps,

N_t = concentration of traps

29

f_{metal}, f_{AlGaN} = occupancy factor for electron states in the metal and AlGaN,

τ_1 = time constant for transfer of an electron between gate metal and traps ,

τ_2 = time constant for transfer of an electron between the traps and the AlGaN.

The first term to the right of the equals sign in Equation 4 describes the number of electrons leaving the metal and becoming trapped per second per unit volume. The second term describes the number of electrons detrapping into the AlGaN per second per unit volume.

We assume that $f_{AlGaN} = 0$, which is reasonable because there are many more empty electron energy states than full states in the conduction band of the AlGaN. We also assume that $n_t \approx 0$, that there are many more empty traps than full traps. Svensson argues that this is a reasonable assumption because the detrapping time is assumed to be very small. In the steady state,

$$\frac{\partial n_t}{\partial t} = 0$$

so that the injected current per unit of gate area over a small interval dx at a distance x into the AlGaN is given by

$$\Delta J = \frac{q N_t f_{metal}}{\tau_1} dx .$$

The total current per unit of gate area is given by

$$J = \int_0^{x_m} \left(\frac{q N_t f_{metal}}{\tau_1} \right) dx \qquad (4)$$

with x and x_m as defined in Figure 13.

30

The time constant for tunneling between a trap and the AlGaN conduction band τ_1 is given by

$$\tau_1 = \tau_0 e^{2\beta x}$$

with τ_0 a time constant on the order of 10^{-12} to 10^{-14} seconds and

$$\beta \approx \frac{\sqrt{2m_{AlGaN} q\phi_t}}{\hbar}$$

with

$$m_{AlGaN} = \text{the effective mass of an electron in the AlGaN}$$

$$\hbar = \frac{h}{2\pi}.$$

The Fermi factor in the metal is approximated by

$$f_{metal} \approx e^{-\frac{qV_t}{kT}}, \tag{5}$$

with V_t equal to the potential at the traps given by

$$V_t = \left(\phi_B - \phi_t\right) - E_j x. \tag{6}$$

Using equations (6,7), equation (5) becomes

$$J = \frac{qN_t}{\tau_0} e^{\frac{-q(\phi_B - \phi_t)}{kT}} \int_0^{x_m} e^{\left(-2\beta + \frac{qE_j}{kT}\right)x} dx.$$

For low temperatures and high fields we obtain, if

$$\left(\frac{qE_j}{kT} - 2\beta\right) \gg 1$$

then

$$I_{TAT} = AJ = \frac{AqN_t}{\tau_0\left(\dfrac{qE_j}{kT} - 2\beta\right)} e^{\frac{-2\beta(\phi_b - \phi_t)}{E_j}} \qquad (7)$$

with A = area of the gate.

Using the simplifying assumption that the potential at the gate is triangular (instead of parabolic), and that $x_m = d$ (the thickness of the AlGaN layer), then

$$E_j = \frac{-\Delta V}{d} = \frac{-Vg}{d} + \frac{\left(-\Delta\phi_c - \phi_{fb} + \phi_b + \dfrac{qN_d d^2}{2\varepsilon_{AlGaN}}\right)}{d}.$$

Equation 8 can be simplified to

$$I_{TAT} = \frac{C_1}{\dfrac{1}{T} - C_2} e^{\frac{C_3}{Vg + C_4}} \qquad (9)$$

with the values of C_1 through C_4 given by

$$C_1 = AN_T \frac{k}{E_j \tau_0} \qquad \left(\frac{mA}{K}\right)$$

$$C_2 = \frac{2\beta k}{qE_j} \qquad \left(\frac{1}{K}\right)$$

$$C_3 = -2\beta(\phi_b - \phi_t)d \qquad (V)$$

$$C_4 = \Delta\phi_C + \phi_{fb} - \phi_b \qquad (V).$$

Note that I_{TAT} has a linear dependence on the density of traps in C_1, so that increasing the number of traps will cause a linear increase in I_{TAT}.

32

Expected values for C_1 through C_4 are given in the following table assuming reasonable values for the independent variables.

Table 1. Expected range of values of STAT parameters C1-C4.

Parameter	Range of Values	Units
C_1	-7×10^{-3} to -2.8×10^{-6}	$\dfrac{mA}{K}$
C_2	-6.9×10^{-5} to -1.7×10^{-4}	$\dfrac{1}{K}$
C_3	-50 to 70	V
C_4	.074 to -.926	V

Table 2. Values of STAT independent variables.

Independent Variable	Values (or range)	Units
A	nominal gate area, 5.0×10^{-9}	m^2
N_t	10^{18} to 10^{22}	$\dfrac{traps}{m^3}$
τ_0	10^{-12} to 10^{-14}	s
E_j	-10^7 to -2.5×10^8 (breakdown voltage)	V/m
β	10^8 to 10^9	m^{-1}
ϕ_b	.5 to 1.5	V
ϕ_t	.1 to 1.5	V
ϕ_{fb}	0.2	V
$\Delta\phi_C$	0.374	V

The voltage dependence of I_{TAT} is shown in Figure 14 for three different temperatures. The values for C_1 through C_4 are taken from Roley's results [7] obtained from IV measurement of neutron irradiated HFETs. Although these values did result in a

good fit to his data, they are not within the expected range of values in Table 1. Roley

used a model fitting routine which was not constrained to reasonable values for

C_1 through C_4.
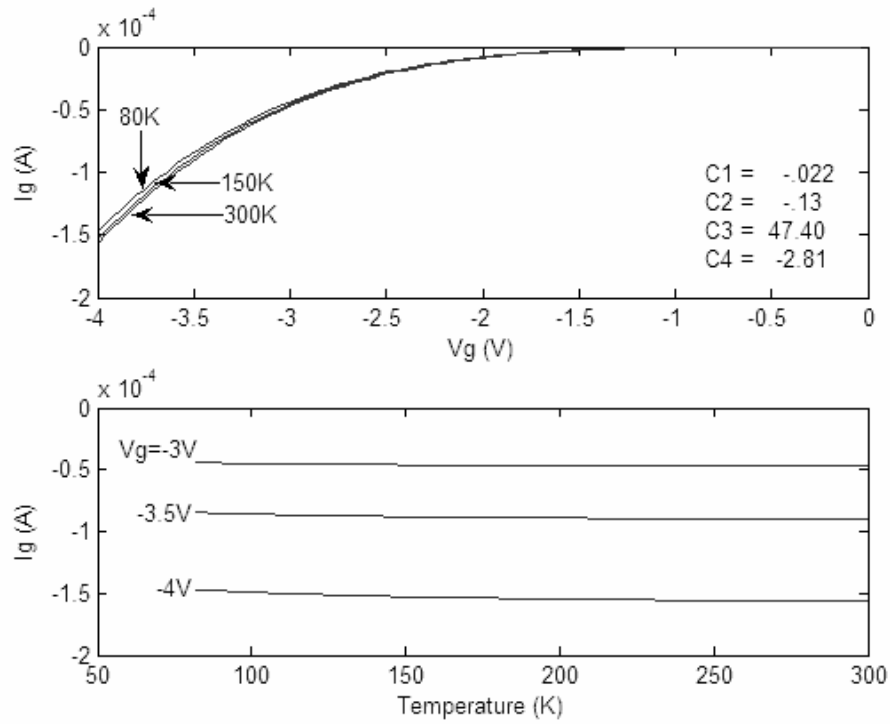
Figure 14. Dependence of I_{TAT} on gate voltage V_g and temperature for STAT model.

The dependence of I_{TAT} on temperature increases with increasing magnitude of

V_g because of the presence of the E_j term in C_1 and C_2. At low bias (up to -3 V) there

is almost no dependence on temperature, while at higher values (-3V to V_{th}) the

magnitude of I_{TAT} increases almost linearly with temperature.

Two methods are presented to solve for the parameters C_1 through C_4. The first

method is to use measured IV and IT data and solve for the parameters directly. A value

is selected for C_4 and C_3, C_2, and C_1 are solved for in order. With four fitting parameters

it is not possible to find a unique solution. The method is:

(1) Select a value for C_4. With $\Delta\phi_C \approx 0.4V$ and $\phi_{fb} \approx 0.2V$ from the Appendix,

and ϕ_B approximately 1.0 V, $C_4 \approx -0.4V$.

(2) Solving equation (9) for C_3 at two different values of Vg at the same

temperature T yields,

$$C_3 = \frac{\ln(|Ig_2|) - \ln(|Ig_1|)}{\dfrac{1}{V_2 + C_4} - \dfrac{1}{V_1 + C_4}}. \qquad (10)$$

(3) Using C_3 and C_4 and measured I_g for two different temperatures at the same

V_g yields,

$$C_2 = \frac{\dfrac{Ig_2}{T_2} - \dfrac{Ig_1}{T_1}}{Ig_2 - Ig_1}. \qquad (11)$$

(4) Using C_4, C_3 and C_2 and a single measurement of I_g at temperature T and

V_g yields,

$$C_1 = \frac{Ig\left(\dfrac{1}{T} - C_2\right)}{e^{\frac{C_3}{V_g + C_4}}}. \qquad (12)$$

Taking the model further, it is possible to predict the value of C_1 and C_2 for a given V_g if the values of C_1 and C_2 are known for two other values of V_g. As previously discussed, C_1 and C_2 have voltage dependence because of the electric field term. The derivation of a method to determine the voltage dependence follows.

With

$$C_1 = \frac{AN_t k}{\tau_0 E_j}, \ E_j = \frac{-\Delta V}{d} = \frac{-Vg}{d} + \frac{(-\Delta\phi_c - \phi_{fb} + \phi_b + \frac{qN_d d^2}{2\varepsilon_{AlGaN}})}{d}$$

let

$$x = \frac{(-\Delta\phi_c - \phi_{fb} + \phi_b + \frac{qN_d d^2}{2\varepsilon_{AlGaN}})}{d}.$$

Then

$$C_1 = \frac{\frac{-AN_t kd}{\tau_0}}{V_g - x},$$

so if $C_1(Vg_1)$ and $C_1(Vg_2)$ are known, it is possible to solve for x in the following manner:

$$\frac{C_1(Vg_1)}{C_1(Vg_2)} = \frac{Vg_2 - x}{Vg_1 - x}$$

$$x = \frac{Vg_1 C_1(Vg_1) - Vg_2 C_1(Vg_2)}{C_1(Vg_1) - C_1(Vg_2)}.$$

With x known, it is possible to solve for $-AN_t kd$;

36

$$\frac{-AN_t kd}{\tau_0} = C_1(Vg - x). \qquad (13)$$

Now it is possible to predict C_1 at other values of Vg.

Similarly, the voltage dependence of C_2 can be solve for:

$$C_2 = \frac{2\beta k}{qE_j}$$

$$C_2(Vg_1) = \frac{\dfrac{2\beta kd}{q}}{-Vg_1 + x}$$

$$\frac{C_2(Vg_1)}{C_2(Vg_2)} = \frac{-Vg_2 + x}{-Vg_1 + x}$$

solving for x,

$$x = \frac{C_2(Vg_1)Vg_1 - C_2(Vg_2)Vg_2}{C_2(Vg_1) - C_2(Vg_2)}.$$

Then

$$\frac{2\beta kd}{q} = C_2(-Vg + x). \qquad (14)$$

Now C_2 can be predicted for other values of V_g.

The second method used to solve for the parameters $C_1 - C_4$ is to build a least squares fitting routine in MATLAB to find values of $C_1 - C_4$ that minimize the least squares fit of the model to the empirical data.

The final method used to fit the STAT model to the data is to do a least squares fit

to the data using ϕ_{bo}, ϕ_t, N_d and N_t as the parameters. As discussed in the next section,

this will allow direct comparison between the STAT model and the Sathaiya TTT model.

The second TAT theory considered was developed by Sathaiya and Karmalkar

specifically to describe trap assisted tunneling currents through AlGaN/GaN

heterojunctions [15,16]. They call their theory thermionic trap assisted tunneling (TTT),

with 'thermionic' indicating the inclusion of thermally activated gate metal electrons in

the model. As with the STAT model, TTT also assumes traps at a single energy ϕ_t below

the AlGaN conduction band uniformly distributed through the AlGaN layer and a

triangular potential at the gate. They find that by including thermally activated electrons

at low electric fields, there is a factor of ten increase in the predicted I_g over the current

predicted by Houng et al. which did not include thermionic electrons. This results in a

better fit to empirical data.

The derivation of TTT is well presented in the Sathaiya paper. A description of

the derivation is presented here in order to compare it with the STAT model.

Sathaiya develops the TTT model based on tunneling probabilities P_1 and

$P_{2\_triangle}$ as shown in Figure 15.
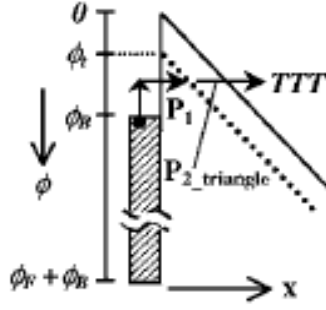
Figure 15. TTT tunneling diagram [18].

As in the STAT theory, ϕ_t is the difference in potential between the AlGaN conduction

band and the traps and ϕ_B is the barrier height. ϕ_F is the amount by which the Schottky

barrier is raised by the gate voltage (in this case, $\phi_F = -V_{th}$).

The TTT current is given by

$$I_{TTT} = \frac{AqC_tN_t}{E_j} \int_{\phi_t}^{\phi_B+\phi_F} \left(\frac{1}{f_{FD}P_1} + \frac{1}{P_{2\_triangle}} \right)^{-1} d\phi .$$

Note that the integral is taken over energy instead of distance as it was in the STAT

model. These limits are equivalent to the STAT treatment because at the gate junction

(x=0), $\phi = \phi_t$, and at x_m (where the metal Fermi level crosses the trap potential)

$\phi = \phi_B + \phi_F$. As noted in the discussion of the STAT model we assume that $x_m = $ d. Also

note that, as with the STAT model, the gate current predicted by the TTT model has a

linear dependence on the density of traps (N_t).

f_{FD} is the Fermi Dirac function for probability of electron occupation of an

energy state at a given potential ϕ in the metal given by

$$f_{FD} = \frac{1}{1 + e^{\left(\frac{q(\phi_B - \phi)}{kT}\right)}}.$$

The tunneling probabilities at energy ϕ are given by

$$P_1 = e^{-\frac{\alpha}{E_j}\left(\phi^{\frac{3}{2}} - \phi_t^{\frac{3}{2}}\right)}$$

and $P_{2\_triangle} = e^{-\frac{\alpha}{E_j}\phi_t^{\frac{3}{2}}}$ with

$$\alpha = \frac{8\pi\sqrt{2m_{AlGaN}q}}{3h}.$$

C_t is a trap energy dependent rate constant given by

$$C_t = \left(\frac{m_M}{m_{AlGaN}}\right)^{\frac{5}{2}} \frac{16\pi q \phi_t^{\frac{3}{2}}}{3h\sqrt{\phi_t - \phi_1}}, \text{ with } \phi_1 = 0.2V \ .$$

With the device biased at the threshold voltage (V_{th}), the electric field and band diagram are modeled as in Figure 16.

E_j is assumed to be constant due to the triangular approximation of the Schottky barrier and given by

$$E_j = \frac{V_P + \frac{qN_d d^2}{2\varepsilon}}{d} \text{ for } |V_g| \leq |V_{th}|,$$

with

$$V_P = -V_g + \phi_B - \Delta\phi_C - \phi_{fb}$$

N_d =donor density in the AlGaN

ε = permissivity of AlGaN.

40
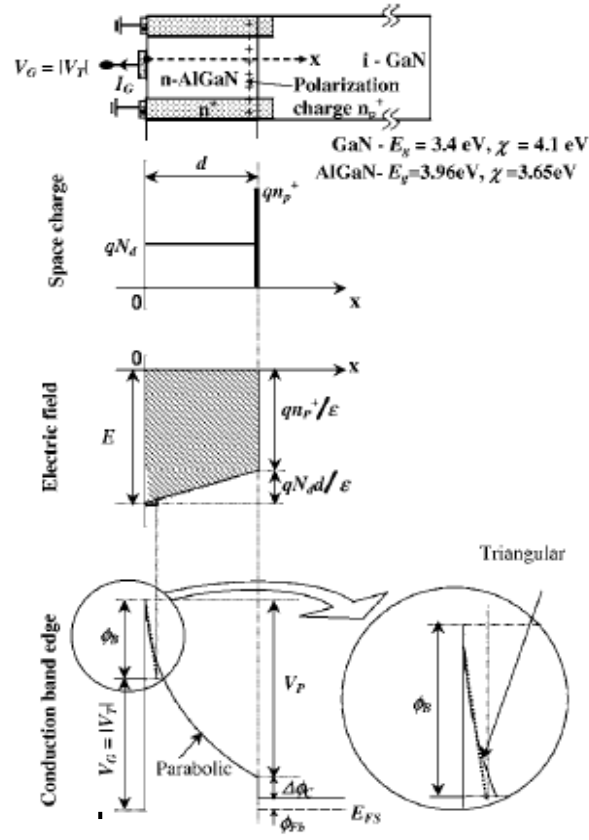
Figure 16. TTT model geometry and energy band diagram at V_{th} [14].

For negative gate voltages greater in magnitude than V_{th} the electric field does not increase beneath the gate because the excess voltage ($|V_g| - |V_{th}|$) drops laterally from the gate to the drain/source.

The effects of image force barrier lowering and AlGaN band gap reduction with temperature are incorporated in the model using

$$\phi_B = \phi_{B0} - \gamma_1 \sqrt{\frac{q}{\pi\varepsilon}} \sqrt{E_j} - \gamma_T T$$

with

γ_1 = image force barrier lowering constant,

γ_T = band gap reduction constant.

A fitted I_{TTT} is calculated by assuming values for the secondary parameters as given in the Appendix and extracting values for the primary parameters ($\phi_{B0}, \phi_t, N_t, N_d$). This is done by incrementally changing the values of the primary parameters until the lowest least squares fit to measured data is obtained.

A MATLAB based numerical integration routine was developed for this experiment based on the TTT model. The TTT numerical integration routine was verified by reproducing a curve published in the Sathaiya paper using values for the primary parameters extracted by Sathaiya. Sathaiya extracted these values for the primary parameters by fitting the TTT model to empirical data [16].

Figure 17 presents an IV curve from the Sathaiya paper (calculated by him using primary parameters fitted to empirical data) and the IV curve produced by the numerical integration routine developed for this experiment. Both IV curves are for 'Device #1' from the Sathaiya paper at 100K and 300K before (1) and after (2) plasma treatment.
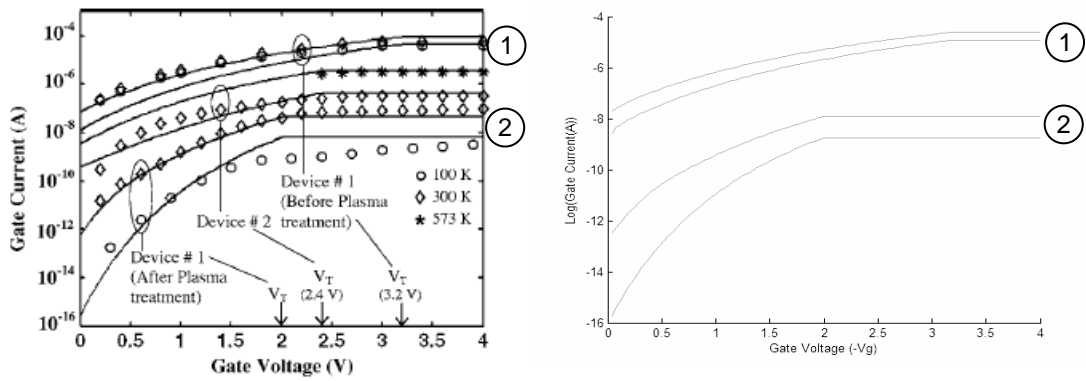
FIG. 7. TTT model fit (solid lines) to experimental data (points) using the parameters given in the Table I, and $m_s=0.17m_0$, $\gamma_1=0.4$, and $\gamma_T=2.7 \times 10^{-4}$ V/K. For device 1, $d=200$ Å and $S=1.1\times100$ μm^2 (see Ref. 7), and for device 2, $d=250$ Å and $S=1\times100$ μm^2 (see Ref. 10). For device 2 at 573 K only saturation data are available in Ref. 10.
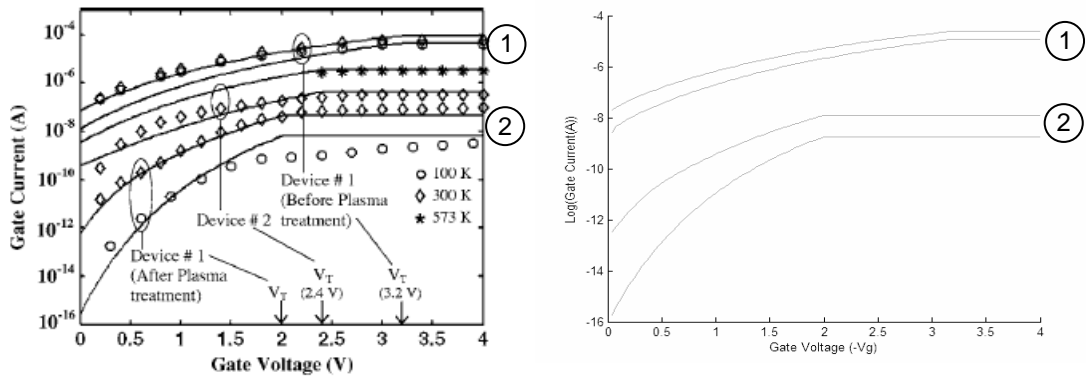
FIG. 7. TTT model fit (solid lines) to experimental data (points) using the parameters given in the Table I, and $m_s=0.17m_0$, $\gamma_1=0.4$, and $\gamma_T=2.7 \times 10^{-4}$ V/K. For device 1, $d=200$ Å and $S=1.1\times100$ μm^2 (see Ref. 7), and for device 2, $d=250$ Å and $S=1\times100$ μm^2 (see Ref. 10). For device 2 at 573 K only saturation data are available in Ref. 10.

Figure 17. TTT model validation against empirical data [16] and MATLAB algorithm calculation. (1) is measured before plasma treatment, and (2) is afterward.

The current predicted by the STAT model was compared with the current predicted by the TTT model. The results are presented in Figure 18, with the temperature in the IV diagram set at 300K and the gate voltage in the lower diagram set at -4V. The

43

values of the primary parameters used in the calculations for both models are listed in

Table 3.
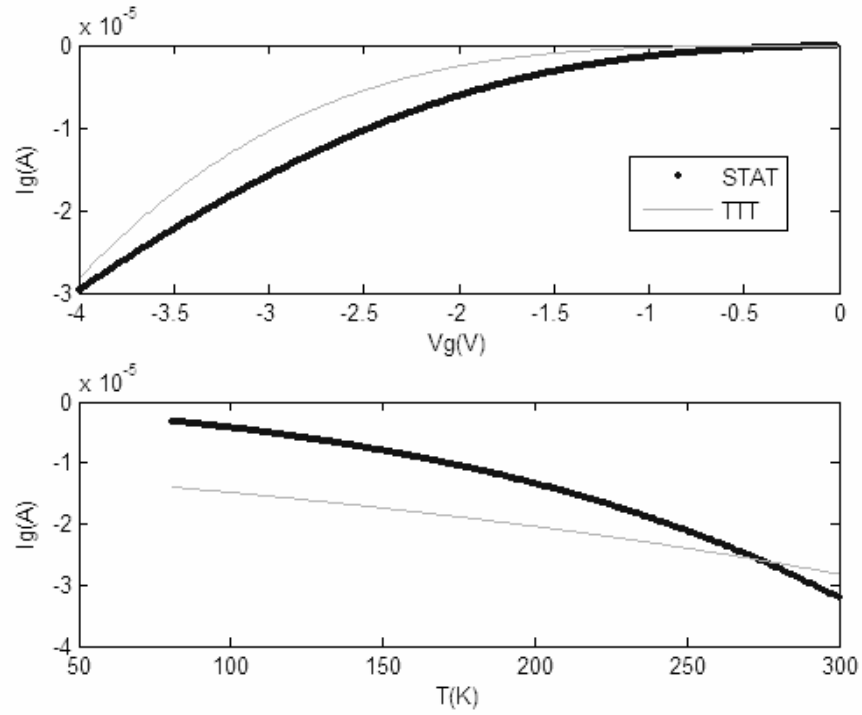
Figure 18. Comparison of TTT calculation with STAT calculation.

Table 3. Primary parameter values used for TTT and STAT model comparison.

Primary parameter	Values	Units
ϕ_b	1.44	V
ϕ_t	.85	V
N_d	4.8×10^{24}	$\dfrac{donors}{m^3}$
N_t	2×10^{22}	$\dfrac{traps}{m^3}$

Both models produce results which are of the same order of magnitude. The TTT model has a more exponential dependence on voltage and a smaller dependence on temperature.

It was found that the value for τ_0 in the STAT model which produced results which were most similar to the TTT model was 2.7×10^{-14} seconds.

Threshold Voltage. For both the STAT and the TTT model the threshold voltage is given by

$$V_{th} = \phi_b - \phi_c - \frac{qN_d d^2}{2\varepsilon_{AlGaN}} - \frac{\sigma d}{\varepsilon_{AlGaN}} \qquad (15)$$

with

σ = sheet charge density at the heterojunction [8].

This expression indicates that a change in Schottky barrier height or donor density will cause a change in V_{th}. This relation will used in the attempt to determining the cause of the increase in I_g after neutron irradiation.

Using the values in

allows us to quantify the expression for V_{th} for the HFETs used in this study. The value for σ was incorrectly reported by Uhlman [8, p. 45] as 0.019 C/m^2. Uhlman used an interpolating formula based on the Al mole fraction in the AlGaN to calculate the sheet charge density. Repeating his calculation identified the error that gave his result. The correct calculated value, using Equation 4 in Uhlman's thesis, is 0.00485 C/m^2. The sheet electron charge density for a .27 mole fraction AlGaN/GaN wafer from the same manufacturer (Cree) as the HEMT devices in this study was measured by Hogsed using

45

hall effect measurement. Hogsed measured a value of 1.1×10^{13} electrons/cm^2, which

when divided by 1.6×10^{-19} C/electron gives the value of σ reported in Uhlman's work.

Hogsed's measured value of σ is assumed to be the best available value and is used for

calculation.

Table 4. Values used for calculation of V_{th}.

Variable	Values	Units
ϕ_c	0.4	V
ε_{AlGaN}	$(9.365)(8.854 \times 10^{-12})$	$\dfrac{F}{m}$
d	25×10^{-9}	m
σ	0.006875	$\dfrac{C}{m^2}$

Using these values results in the following expression for V_{th},

$$V_{th} = \phi_b - (6.03 \times 10^{-25})(N_d) - 2.5 \text{ V} . \qquad (16)$$

TTT dependence on ϕ_b and N_t. In order to predict the change in IV and IT

curves we should expect after neutron irradiation it is useful to observe the change in the

TTT model IV and IT curve characteristics with changes in ϕ_b and N_t. The baseline

curves in Figure 19 are based on the values in Table 4 above. Figure 19 indicates that

either a decrease in ϕ_b (from 1.44 V to 1.34 V) or an increase in N_t (from 2.0×10^{22} to

$2.5 \times 10^{22} \dfrac{traps}{m^3}$) will have the same qualitative result. The IV curve bends more sharply

and the IT curve is translated further down the graph without a noticeable change in

shape or tilt. The lack of qualitative change in the IV or IT curves suggests that they may

be of limited use in determining the cause of increased I_g after irradiation.
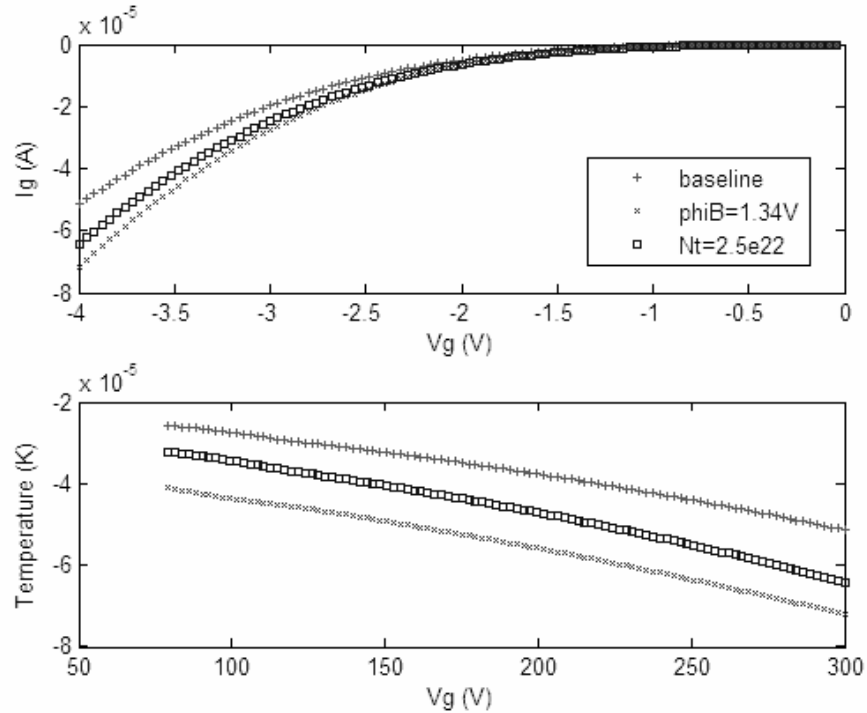
Figure 19. Change in IV and IT due to change in ϕ_b or N_t.

Sensitivity Analysis

    The sensitivity, S, of current to changes in the variables in each of the models was

analyzed using the method developed by Petrosky [19],

$$\frac{\Delta I_G(y)}{I_G} = S \frac{\Delta y}{y}.$$

    The value of S indicates the relative importance of each of the variables in

determining the current. In addition, a high sensitivity of current to a given variable

determines how precisely that variable must be measured during experiment in order to

47

provide useful results. S is found by incrementally changing the value of one variable

while holding the other variables constant. The ranges of values used for each variable

are indicated in the following discussion of my analysis of each model.

 TE Model. The sensitivity of I_{TE} is given in Table 5.

Table 5. Sensitivity of TE model.

Variable	Range Considered	S
A	0.25 x 10^{-9} to 0.75 x 10^{-9} m^2	1
A*	6 x 10^4 to 6 x 10^5 $\dfrac{Amps}{m^2 K^2}$	1
ϕ_b	0.02 to 1.58 Volts (For T =77 to 300 K)	-6 to -12,000
T	77 to 300 K (For ϕ_b =0.02 to 1.58 Volts)	15 to 32

 The sensitivity of ϕ_b and T show a great deal of interdependence. In the low

temperature regime, with an expected ϕ_b of approximately 1.33 V, the current will have

the greatest dependence on ϕ_b.

 FE Model. The sensitivity of I_{FE} is given in Table 6. I_{FE} has the greatest

dependence on ϕ_b. The dependence of S(ϕ_b) on temperature and S(T) on ϕ_b are similar

to the TE model.

Table 6. Sensitivity of FE model.

Variable	Range Considered	S
A	0.25×10^{-9} to 0.75×10^{-9} m^2	1
A*	6×10^4 to 6×10^5 $\dfrac{Amps}{m^2 K^2}$	1
m*	0.2 to 0.35 m_e	-0.06 (T=77K) 0.07 (T=150 to 300 K)
N_d	10^{11} to 10^{21} donors/cm^3	0.45 to 1.1
ε_s	8.27 to 8.31 x 10^{-11} $\dfrac{C}{mV}$, corresponding to an Al mole fraction between 0.22 and 0.32.	0.07 to .1
ϕ_b	0.2 to 1.2 Volts	-125 to -4x10^7
T	77 to 300 K	10 to 27

STAT and TTT Models. The sensitivity of I_{TAT} is given in

under the conditions given in Table 7.

Table 7. Sensitivity of STAT and TTT models.

Variable	STAT	TTT
ϕ_b	-53.0	-10.4
ϕ_t	10.0	-6.0
N_d	1.9	2.2
N_t	1.0	1.0
T	3.0	1.0
Vg	2.5	2.9

The greater dependence on T in the STAT model is apparent in Figure 18, as is

the smaller dependence on V_g compared with the TTT model. I_g increases with

increasing ϕ_t in the STAT model and decreases with increasing ϕ_t in the TTT model.

This is an unexpected result and may be due to the simplifying assumption that x_m is

equal to the thickness of the AlGaN in the STAT model. Both models show a linear

dependence on trap density, as expected.

III. Equipment and Procedure

Equipment

The neutron irradiation experiments took place at the Ohio State University Research Reactor (OSURR). The OSURR is an enriched U^{235} reactor surrounded by a 20 foot deep pool of water. The pool provides cooling, neutron moderation, and gamma shielding. Roley's results were obtained at the same reactor but he had great difficulty controlling temperature and achieving safe reactor operation because he was working with the reactor's horizontal 'rabbit tube' and horizontal beam port. In order to avoid this problem a vertical irradiation chamber was built and installed for this experiment. The basic configuration is shown in Figure 20.
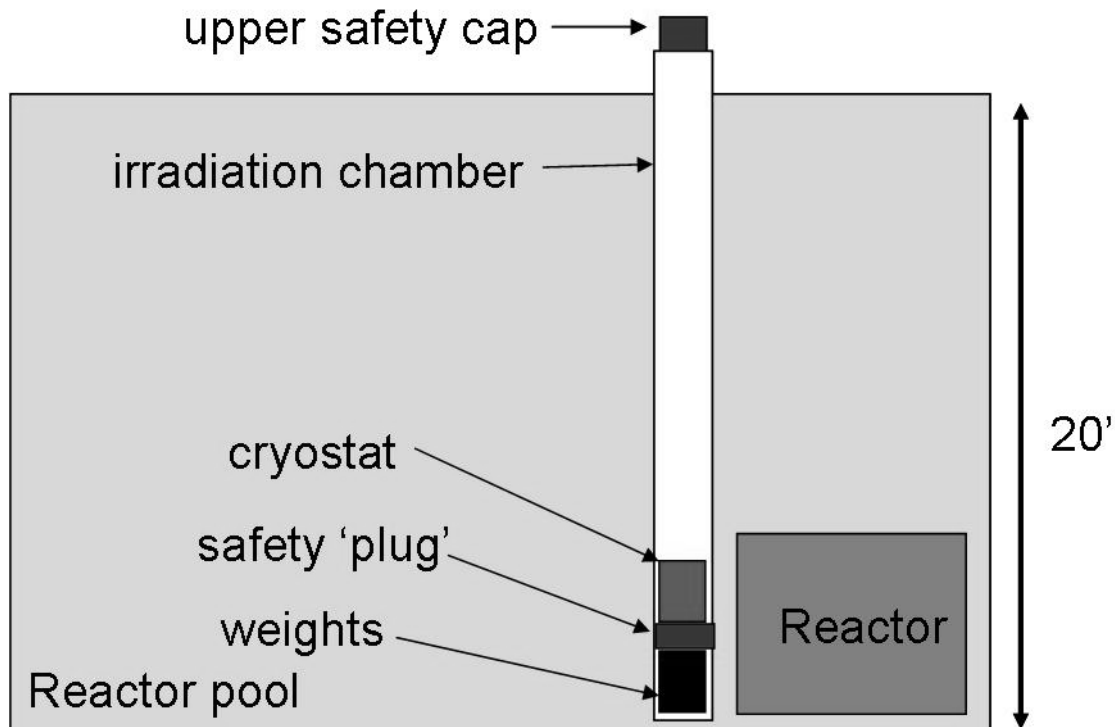

Figure 20. Configuration of OSURR reactor and irradiation chamber.

<u>Irradiation Chamber</u>. The irradiation chamber consisted of a 20.5' long, 7" outside diameter 6061 T6 aluminum tube with walls .125" thick. Approximately 350 pounds of soft steel weights were machined to provide negative buoyancy.
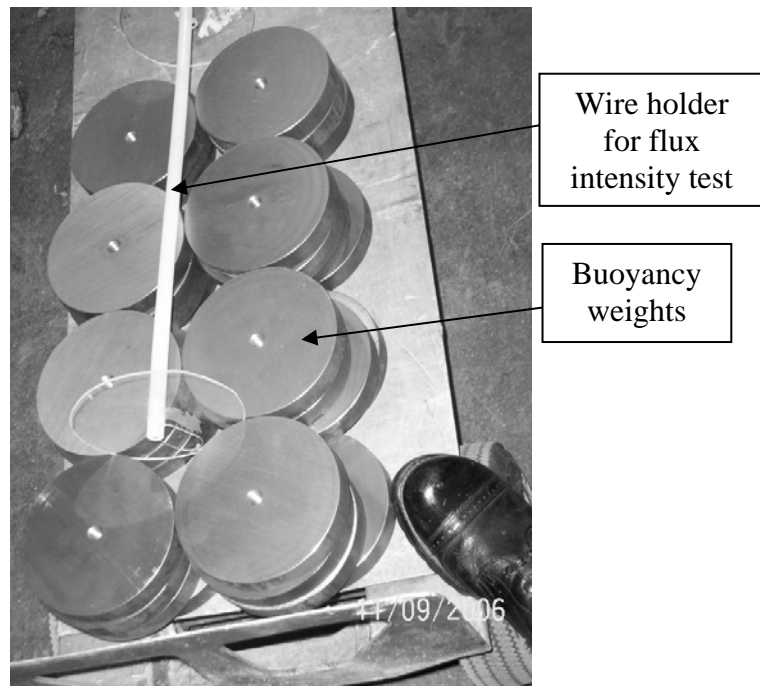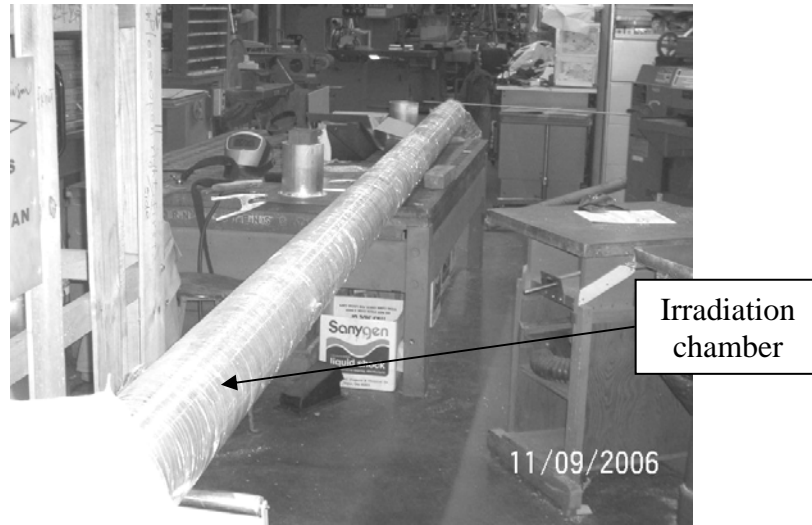

Figure 21. Irradiation tube and buoyancy weights.

The irradiation chamber was lowered into the reactor pool using an overhead crane (Figure 22). Weights were added until the chamber had a negative buoyancy of approximately 15 pounds. The chamber was moved into contact with the reactor with the top of the chamber tube against a bracket during each experiment. This ensured that the fluence through the chamber was the same for each irradiation. Between experiments the chamber tube was moved to the end of the pool furthest from the reactor for storage.
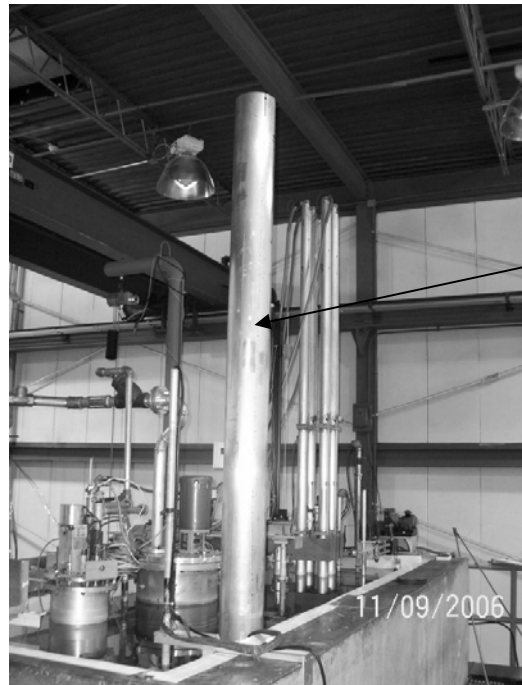
Irradiation chamber being lowered

Figure 22. Installing irradiation chamber.

Figure 23. Irradiation tube positioning bracket.
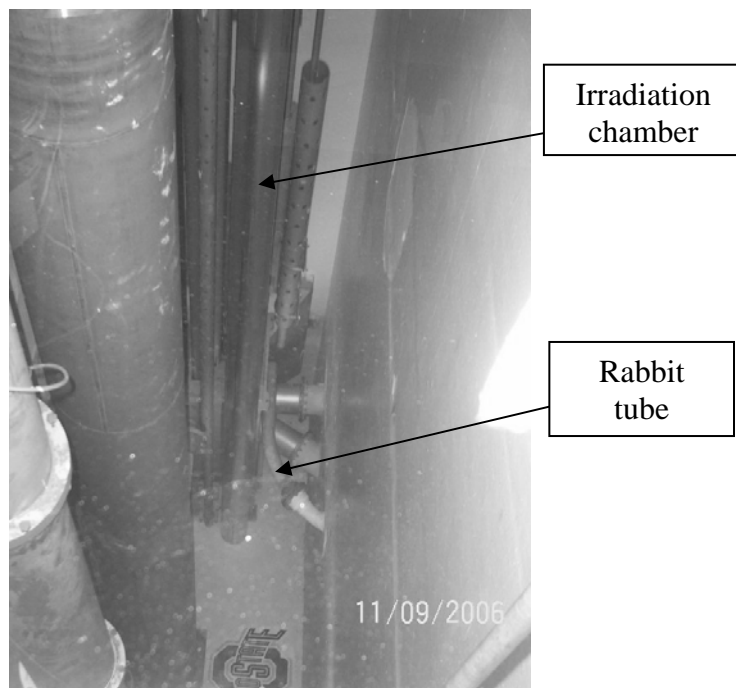
Figure 24. Irradiation tube placement against reactor.

The top cap was designed to reduce the streaming radiation coming up through the irradiation chamber. It consists of, from bott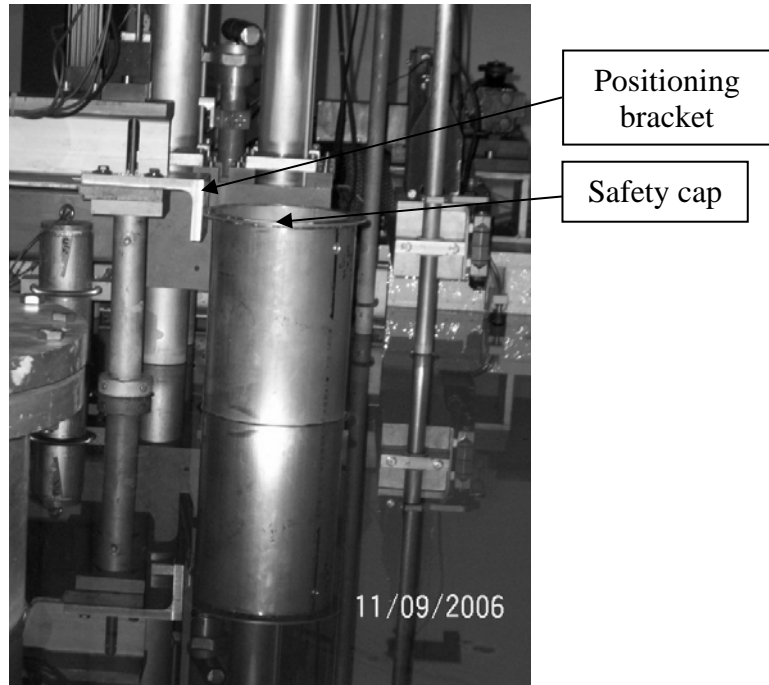om to top, 5 one-inch layers of high density polyethylene, 0.025" of cadmium, and approximately 0.75" CerroBend Aim 70 (Figure 26). The polyethylene has a high hydrogen content and moderates neutrons. The cadmium absorbs the moderated neutrons. The CerroBend contains high atomic mass material (mostly bismuth with some lead, cadmium and tin) and absorbs gamma and x-rays. The holes in the cap and shielding materials shown in Figure 25 and Figure 26 were intended to allow the cryostat to be refilled with liquid nitrogen and to allow data to be taken without removing the cryostat from the irradiation tube. This feature was not used in this research but is available for future work.

Figure 25. Safety cap without moderators or absorbers.

High density polyethelene neutron moderators

CerroBend gamma absorbers

11/09/2006

Figure 26. Safety cap moderators and absorbers.

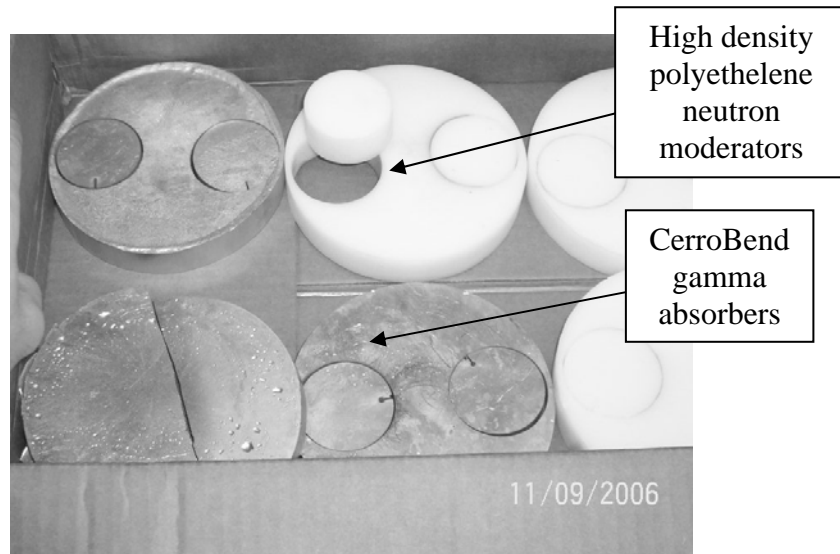Cryostat. A cryostat was designed for this experiment. A previous cryostat, used by Roley, consisted of a glass dewar enclosed in an aluminum housing. The cryostat laid on its side in the rabbit tube during the experiment. The dewar broke during irradiation, perhaps because of the difference in thermal expansion between the glass and the aluminum housing, and liquid nitrogen was released in the rabbit tube. In order to avoid this danger an all aluminum cryostat was designed.

The cryostat consists of outer and inner cylinders between which a vacuum was maintained in order to prolong the life of the liquid nitrogen coolant (Figure 27).

The outer cylinder was covered in Cd to absorb thermal neutrons. The inner cylinder acts as an aluminum dewar containing liquid nitrogen at the bottom of which was attached a fin to which are attached the HFETs and temperature sensor. In the end of the fin a hole was bored to accept a resistive heater as a press fit. A sheet of lead was placed next to the fin to shield the HFETs from gammas in order to reduce photocurrent.

The top of the outer cylinder contains pass-throughs for coaxial cable connectors and fill and vent ports for the dewar. The cylinders and as much of the hardware as possible were made of 6061-T6 aluminum which is low in elements with large activation cross sections (Cr, Cu, Fe, Mn, Zn).
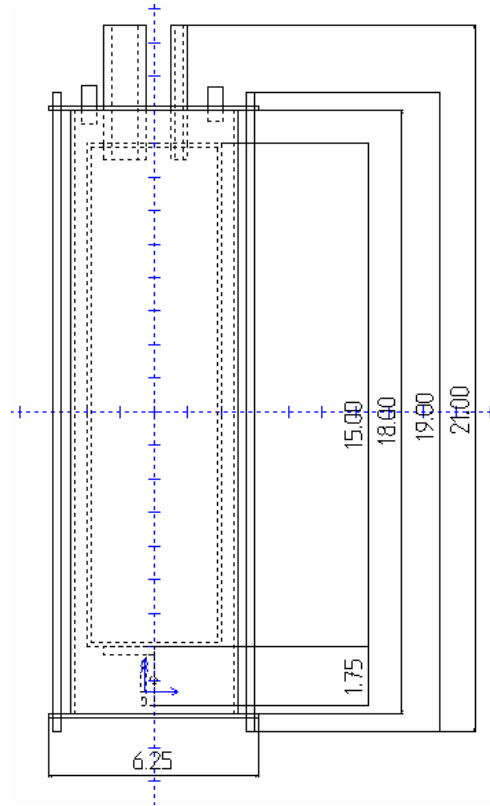
Figure 27. Cryostat assembly drawing. Measurements in inches.
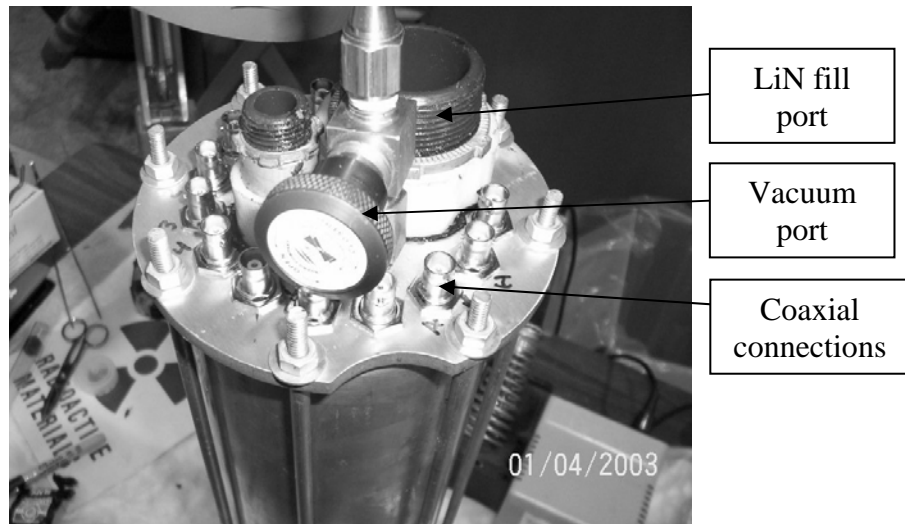
Figure 28. Cryostat body and top cap, showing ports.

A rough thermodynamic calculation predicted that the HFETs would be

maintained close to liquid nitrogen temperature for over two hours if a vacuum could be

maintained in the cryostat. However, vacuum could not be maintained because of

imprecision in the placement of the liquid nitrogen fill and vent ports. The ports were

placed at a slight angle to each other which made it impossible to maintain a vacuum tight seal when liquid nitrogen was added. The lifetime of the liquid nitrogen was limited to one hour and some data was taken using the device. Most data was taken using a simpler apparatus which will be described next.

When the aluminum cryostat proved to be ineffective, a simpler method was developed. The devices were affixed to aluminum fins which were held upright in a glass dewar filled with liquid nitrogen. Thermocouple temperature sensors were attached to the fins through the end of which resistive heaters had been inserted (Figure 29). A portion of the fin below the devices was milled to approximately 0.03" to reduce the rate at which heat was conducted away from the devices and enable the 5 watt heaters to provide a greater temperature range. The devices, sensors, and heaters were surrounded in Styrofoam and wrapped in fabric tape to reduce temperature change due to convection. The fins were placed upright in a glass dewar of liquid nitrogen, with the devices at the top. The dewar and devices were then wrapped in cadmium and lowered into the irradiation chamber.
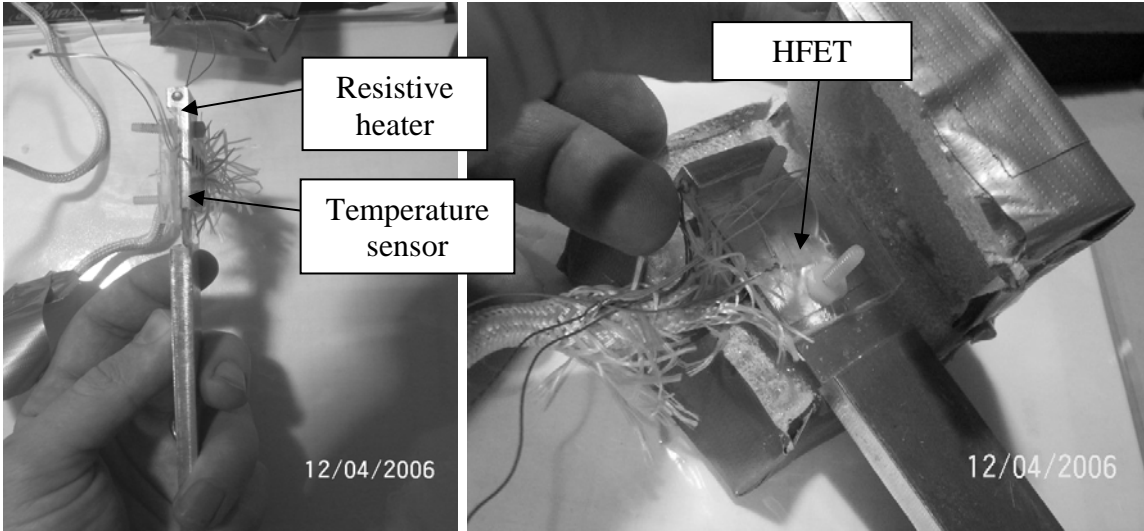
Figure 29. Aluminum fin, heater and temperature sensor.

Data was taken using a laptop computer running LabView 7.0 which controlled

two Keithly 237 source measurement units (SMUs) and a LakeShore 331 autotuning

temperature controller (ATC) through a general purpose interface bus (GPIB) (Figure

30).

Figure 30. Laptop and measurement equipment.

Equipment Issues

After all data was taken it was discovered that SMU #17 had a defect that caused it to source voltage incorrectly. This defect was not identified during the equipment calibration conducted before the experiment because the SMU performance was not tested at a high enough current. The SMUs have three separate circuits for sourcing voltage and reading current. Each circuit is designed to give the best possible precision in their respective current ranges. These are identified as the 0.1, 1 and 10 mA ranges in the users manual. The SMUs were operated in 'autoranging' mode which caused them to automatically switch from one range circuit to another when the measured current crossed the range threshold. Using the 1 mA range in SMU #17 sources a voltage which is higher by a factor of approximately 1.60 compared to the voltage specified on the front panel. An example of the resulting IV curve, for a 767 ohm resistor, is shown in Figure 31.
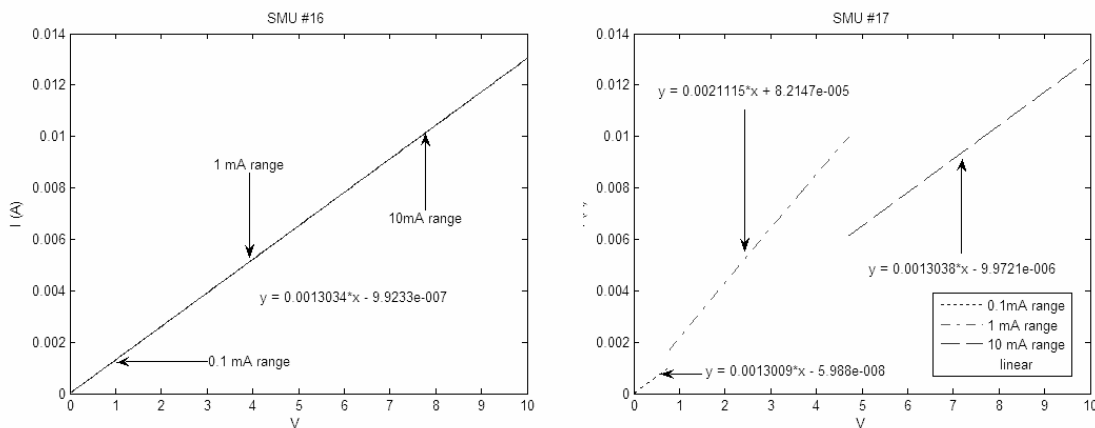

Figure 31. Resistor IV curves from SMU #16 and SMU #17 .

Both SMUs produced R^2 values of over 9.99999 for the transistor data shown in the figures. The slope of the lines in the 0.1 mA and 10 mA ranges indicate that SMU #17 agrees with SMU #16 to within less than 0.2%. The slope of the 1.0 mA range of SMU #17 indicates a resistance of 473.5 Ohms instead of the 767.2 Ohms indicated by SMU #16 and the 0.1mA and 10mA ranges of SMU #17. For simple devices like transistors this IV data could be corrected. However, the IV response of HFETs is much more complex than that for a resistor and in most cases data was invalidated because the voltage desired (i.e. -4.0 V, before V_{th}) was not the voltage sourced (-4.0 x 1.60 = -6.40 V, beyond V_{th}). The use of data taken with SMU #17 is addressed in the results section.

Procedure

The procedure used was to pre-characterize the HFET devices, irradiate them with neutrons at varying fluence levels, and measure the temperature dependent gate current at various negative gate voltages. The voltage and temperature dependence of the gate current was then analyzed to discover the mechanism responsible for producing the gate current.

HFET preparation. The HFETs were grown by Cree, Inc using metal-organic vapor-phase epitaxy [8]. The HFETs were cut from the wafer and affixed to open faced mounts by the Air Force Research Lab (AFRL/SNDD) at Wright Patterson Air Force Base, Ohio.

Some devices (A15, A16, A21, A23 A1, A14) had their surfaces cleaned using acetone. The procedure used was to place several drops of acetone on the open face of the HFET using a syringe. The acetone was allowed to remain on the HFET for 20

minutes, during which time additional acetone was added to keep the surface covered. After 20 minutes the excess acetone was removed and the HFET was dried by fanning air against it. Many of the devices were damaged by the acetone. Further investigation revealed that the procedure used by AFRL/SNDD called for an 8 second cleaning. As a result of the long contact with acetone the transistor action of the HFETs was destroyed, although the IV and IT characteristics of the gate current was only slightly changed. Only HFET A16 produced usable data.

It was discovered that the HFETs were very sensitive to current surges produced by static electricity. Several devices were destroyed because they were stored in a plastic bag with their leads exposed. Storing them separately in plastic bottles with screw on lids eliminated the problem.

Pre-characterization. The voltage and temperature dependent gate currents of each device were measured using the same equipment, cables, and configuration used for the irradiation experiments. The intent of pre-characterization was to ensure that the equipment was able to take data with the required degree of precision and to record pre-irradiation IV and IT curves for analysis and comparison after irradiation.

The voltage dependence of the gate current was measured using an SMU. The gate was connected to the 'output high' terminal and the source and drain were tied together and connected to ground. The LabView program then took an IV curve between 0 and -6 V using the SMU sweep function. The current recorded at each voltage was the average of 32 measurements. IV curves were taken for all HFETs at room temperature

and at various temperatures between 77K and 300K as controlled and measured by the Lakeshore ATC.

The temperature dependence of the gate current was measured using the same configuration as for voltage dependence. In addition, the HFETs were affixed to the end of an aluminum fin (Figure 29) for either the aluminum cryostat or the glass dewar method. Once the temperature sensor indicated that the temperature had stabilized at the lowest achievable temperature, which was normally around 85K, the LabView program was used to control the Lakeshore temperature control unit and raise the temperature. The Lakeshore was directed to raise the temperature by increments of 1K. The LabView program caused the SMU to set voltages between -1.0 and -4.0 V (with 0.5 V increments) and measure gate current when the temperature sensor indicated a temperature within 0.25K of the goal temperature. The temperature control unit frequently maintained the temperature to within a few hundredths of a degree K of the goal temperature. LabView then wrote the data to an Excel file and directed the temperature control unit to raise the temperature to the next setting. For some HFETs IV curves were taken at intervals of 30K in order to examine the temperature dependence of the 'tail' beyond the threshold voltage cutoff.

Transistor curves were taken on all HFETs at room temperature to ensure that they were working correctly. The gate of each HFET was connected to the 'output high' of the top SMU in Figure 30. The source of the HFET was connected to the 'output high' of the bottom SMU. The ground of both the top and bottom SMUs were connected to the HFET drain. The Labview program caused the top SMU to set the gate voltage (0.0

to 4.0 V with 1.0 V increments) while the bottom SMU swept a voltage between 0.0 and 4.0 V (0.1 V increments) and measured source to drain current.

Irradiation. HFETs were held at approximately 85K in the cryostat (or dewar) and irradiated to varying fluence levels in the irradiation chamber. Within 15 minutes of irradiation the HFETs were removed from the chamber. HFETs tested using the cryostat were measured by connecting coaxial cables to the cryostat. HFETs connected to aluminum fins and tested using the glass dewar were measured by removing the fins from the dewar and immediately placing them in another dewar of liquid nitrogen. This was done in order to reduce the operator's exposure to the gammas produced by activation of the dewar (primarily the silver). Connections were made to the HFETs using coaxial-to-alligator-clip connections. IV and IT data was then taken using the same method used for pre-characterization.

Dosimetry

The flux profile at the bottom of the irradiation chamber was measured by irradiating a copper wire, held vertically in the bottom of the chamber by the device in Figure 21, and measuring the activity of segments of the wire at one inch intervals. The flux profile is given in Figure 32.
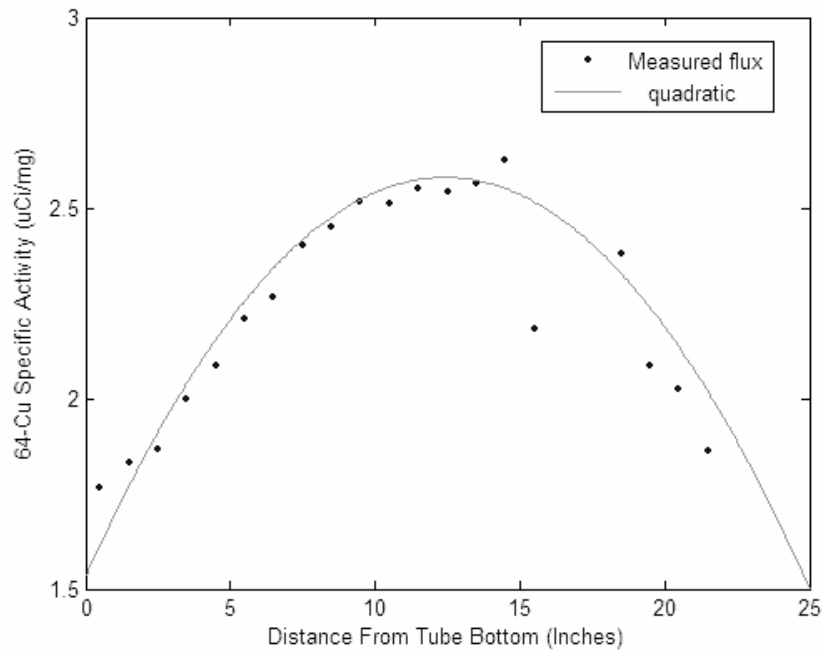
Figure 32. Irradiation chamber neutron flux profile.

A distance of 13 inches from the bottom of the tube was selected in order to maximize the neutron flux. All irradiations were made with devices at this position.

The neutron spectrum was measured by activation analysis. Gold, copper and cobalt wires were irradiated at the position where the devices were to be attached on the fin in the cryostat. The cryostat was wrapped in cadmium and placed at the same position in the irradiation chamber that would be used for the experiment. One set of wires was bare and the other set was enclosed in cadmium. The reactor was run for one hour at 50kW. The wires were removed and their activities were counted using a high purity germanium gamma detector.
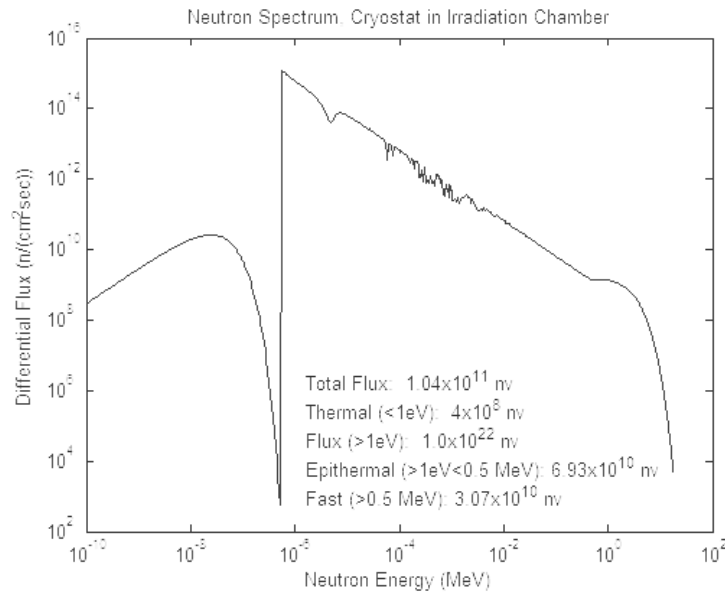
Figure 33. Neutron spectrum inside the cryostat.

At 450kW power, a neutron flux of 3.07×10^{10} n/cm²-s of >0.5 MeV neutrons was measured. Neutron flux is linearly proportional to reactor power. The fluence used in this experiment is given in Figure 33. Because of uncertainty in the measurement of the spectrum the fluence has an error of greater than 25%.   For the purpose of this experiment, however, what is important is the reproducibility of the neutron damage effect on the HFETs for each irradiation, which is estimated to have an error less than 10%, primarily due to uncertainty in the orientation of the HFETs in the irradiation chamber.

The fluence used in this experiment, based on times of irradiation and reactor power, are at Table 8.

67

Table 8. Calculated fluence of >0.5 MeV neutrons.

Power (kW)	Time (minutes)	Fluence (n/cm^2) (+/- 25%)
1	10	4.1×10^{10}
10	10	4.1×10^{11}
40	10	1.6×10^{12}

V. Analysis and Results

Chapter Overview

The uncertainty in measurement is quantified and the pre-irradiation IV and IT data is presented. The TE, TFE and surface leakage models are considered and the STAT and TTT models are shown to give the best fit to data. The TTT model is used to investigate the increase in current after neutron irradiation.

Uncertainty

The Keithly Source Measure Units 237 (SMUs) specifications state that they have less than a 0.04% error in both sourced voltage and measured current. The reproducibility of measurements on the HFET devices was tested by measuring IV curves of gate current. Ten IV curves were taken by sourcing voltages between 0.0 and -8.0 V at 0.1V intervals and measuring current at each voltage, for a total of 800 data points. The SMUs were powered down between measurements and the connections between the SMUs and the HFETs were disconnected and reconnected. The maximum uncertainty was $\pm 3\%$, which is taken to be the uncertainty in current measurement for the following data.

The Lakeshore 331 Autotuning Temperature Controller specifications using a thermocouple vary between ± 406mK at 4.2K and ± 110mK at 300K. For measurements in which the temperature was held static, such as IV measurements, the Lakeshore unit indicated that the temperature varied by less than 0.1K. During IT measurement the LabView program directed the SMUs to take data when the temperature was within

0.25K of the target temperature. Therefore the known uncertainty in temperature is

± 0.1K for IV measurements and ± 0.25K for IT measurements. There is a further

unknown uncertainty in temperature measurement because of temperature gradients

across the thickness of the aluminum fin, and the possibility that the HFETs were

receiving thermal loading from the outside environment through the insulating package.

An attempt was made to minimize these effects by varying temperature slowly and by

maintaining a low temperature environment around the insulating package by using a

large glass dewar during measurement. The large dewar permitted the insulating package

to remain below the top of the dewar in a cold nitrogen atmosphere.

Precharacterization IV and IT curves

      Two sets of HFETs were used in this study. The first set, from which only the

data from device A16 is presented, was fabricated from the section of the Cree wafer

identified as JS01A by Uhlman [6], at the same time as Uhlman and Roley's HFETs were

fabricated. The second set of HFETs, identified as G1, G2, G3 and G4, were cut from the

section of the Cree wafer identified as JS01B approximately three weeks before this work

took place. The G1-G4 set was mounted in the same type of package and the gate, source

and drain were connected to the package in the same manner as the HFETs used by

Uhlman and Roley.

      The first set of HFETs , which originally included five HFETs, had an almost

linear gate current dependence on temperature (IT curves). The second set showed much

more complex behavior in the IT curves. Both sets showed similar behavior in the IV

curves. The cause for the differing characteristics between the sets is unknown, but it is

suspected that the portion of the wafer from which the second set was taken had undergone a passivation process. Because of the simpler behavior of the first set of HFETs, device A16 will be used to investigate the mechanism responsible for gate current and the mechanism responsible for increased gate current after irradiation.

Figure 34 shows pre irradiation IV and IT curves for device A16, which are typical of the first set of devices. The voltage dependence and temperature dependence clearly resemble the predictions of the STAT and TTT models.
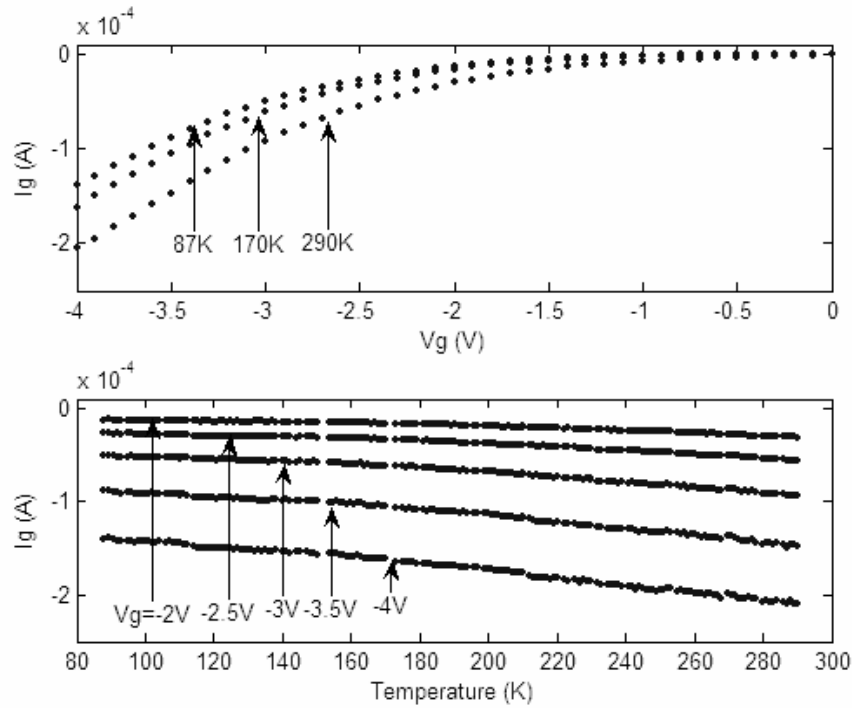

Figure 34. HFET A16 pre irradiation IV and IT data.

Attempts to fit the TE and TFE models reveal that no realistic combination of variables results in curves that resemble the data, which is consistent with the results demonstrated by Uhlman [6]. Furthermore, IV data taken beyond the assumed threshold voltage shows a distinctive change in character at what appears to be the threshold

71

voltage. This is identified in Figure 35 as approximately 4.3 V for HFET A16. The definition of threshold voltage in the TTT and STAT models requires that the gate current saturate. It is evident from Figure 35 that the gate current does not saturate, but instead continues to rise as though a resistive mechanism were added to the expected saturation current (1.5×10^{-4} A at 87K, 2.5×10^{-4} A at 270K). There is insufficient data to determine whether the point where the gate current stops following the trap assisted tunneling model and takes on a resistive character is truly the threshold voltage. Furthermore, assuming the break in the curve is V_{th}, the break is not sharp enough to indicate the value of V_{th} unambiguously. Measuring V_{th} by setting a source to drain voltage and increasing the magnitude of the gate voltage to cut off the source to drain current also produces a curve which gives an ambiguous value for V_{th}. When measured in this manner, the cutoff voltage is identified as the voltage 'where the source to drain current becomes negligible'. This is ambiguous in that the amount of current is not defined. The question could be settled by specifying an ad hoc value for the source to drain current. However, as no further data is available in this research effort, the break in the gate current IV curves will be assumed to represent V_{th}, and the value of V_{th} will be estimated by eye.

The presence of the (assumed) saturation of the gate current is predicted by the architecture of the HFETs. The unexpected appearance of a resistive 'tail' beyond the threshold voltage suggests surface leakage. However, if the mechanism responsible for the increased current beyond V_{th} is due to a resistive term (such as surface leakage), then we would expect that it would also contribute current at lower values of V_g. The data

72

indicates that this is not the case, because the resistive term would contribute much more
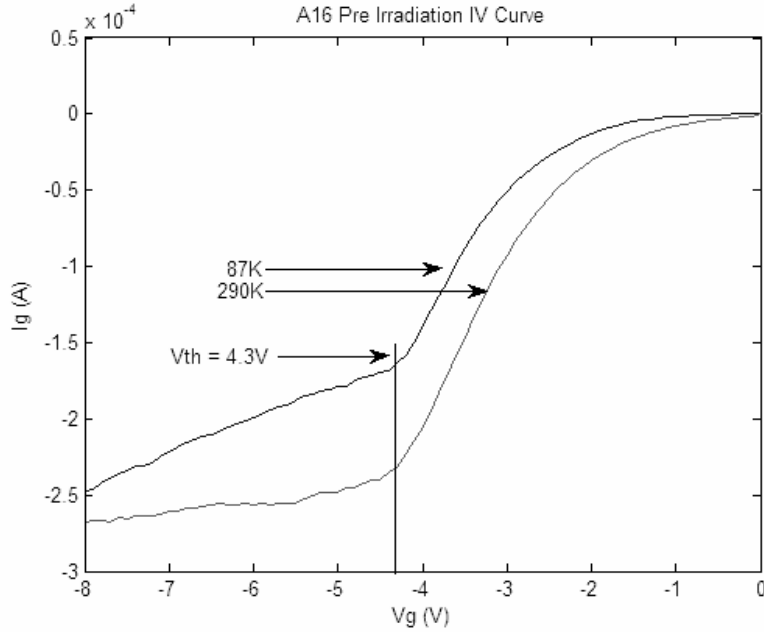current that the data indicates at low values of V_g.

Figure 35. HFET A16 pre irradiation IV curve.

The temperature dependence of the 'tail' is also an interesting feature (Figure 36).
In the case of HFET A16, the slope remained almost constant from 87K to 270K, and
then decreased with increasing temperature indicating that the unknown mechanism
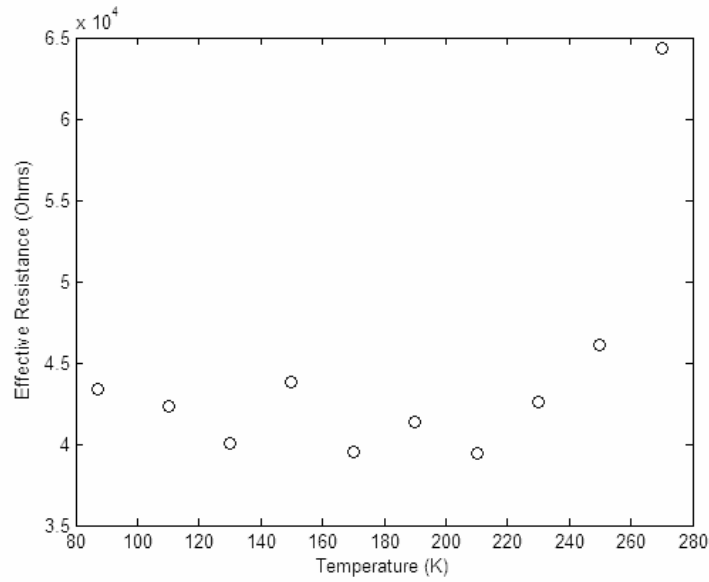became more resistive as temperature increased.

Figure 36. HFET beyond threshold resistive mechanism temperature dependence.

Fitting STAT model to A16 pre irradiation data.

Using the STAT fitting methods discussed in the theory section results in a good qualitative fit to the measured data. The values of C1-C4 in Table 9 are calculated using formulas (10), (11) and (12) and the data from device A16.

Fit	-4V	-3.5V	-3V
C1	-0.00002225	-0.00001469	-0.00000989
C2	-0.01243422	-0.00849719	-0.00596698
C3	8.82918543	8.82918543	8.82918543
C4	-0.40000000	-0.40000000	-0.40000000

Table 9. Extracted STAT model parameters (C1-C4).

Using C_1 and C_2 at V_g = -4V and -3.5V enables prediction of the value of C1 and

C2 at V_g = -3V using formula (13) and (14).

C_1 variation with V_g		C_2 variation with V_g	
x	4.973	x	5.079
$\dfrac{-AN_t kd}{\tau_0}$	-2.164E-05	$\dfrac{2\beta kd}{q}$	-1.342E-02
$C_1(Vg=-3V)$	-1.097E-05	$C_1(Vg=-3V)$	-6.454E-3

Table 10. Predicted STAT C1 and C2 values at Vg = -3.0V.

Using the predicted values of C1 and C2 at Vg = -3.0V results in good fit to empirical

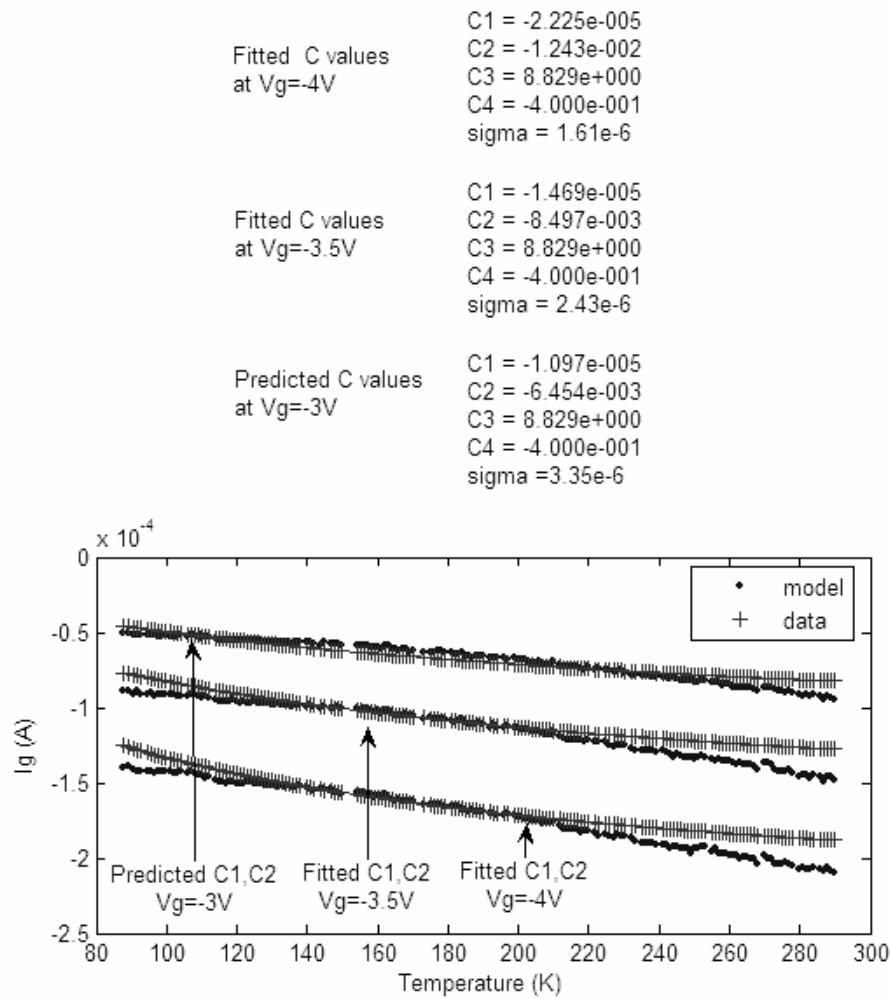data, as shown in Table 10 and Figure 37.

Figure 37. STAT model fit to HFET A16 using both fitted and predicted C1-C4.

The second method used to fit the STAT model to data is a least squares routine in MATLAB. The routine was only able to fit at one value of V_g on the IT plot because the fitting routine treats C1-C4 as constants and does not account for the C1 and C2 dependence on field (and on Vg). The result is shown in Figure 38.
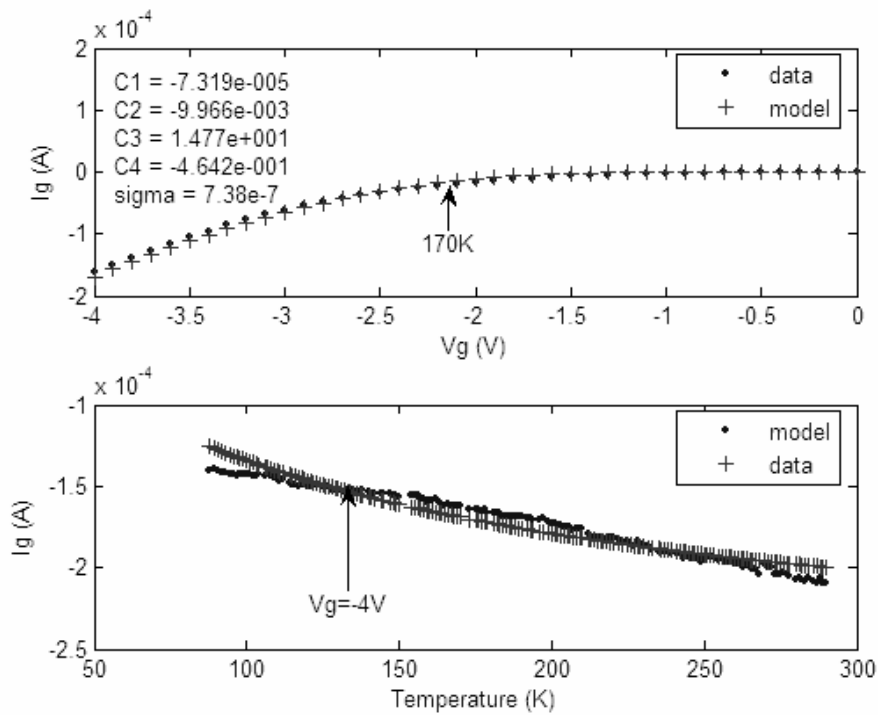
Figure 38. STAT model fit to HFET A16 using least squares.

Fitting TTT model to A16 pre irradiation data.

Fitting with the TTT model results in a greatly improved fit to both the IV curves at multiple temperatures and to IT curves at multiple values of Vg (Figure 39). Note that the values of the primary TTT model parameters ϕ_b, ϕ_t, N_d and N_t presented on the TTT model figures are not intended as accurate measurements of the physical values of those variables. Instead, these values demonstrate that one combination (possibly out of many combinations) of physically reasonable values of those four primary parameters provides a good fit to the measured data. If it becomes possible to measure a given parameter, such as ϕ_b, independently, then the possible values of the other parameters will be constrained. The ability of the TTT model to predict I_g with more constraint on the

77

values of the primary parameters will indicate how completely the TTT model describes

the physics of I_g. One such constraint, discussed earlier, is the relation between V_{th}, ϕ_b

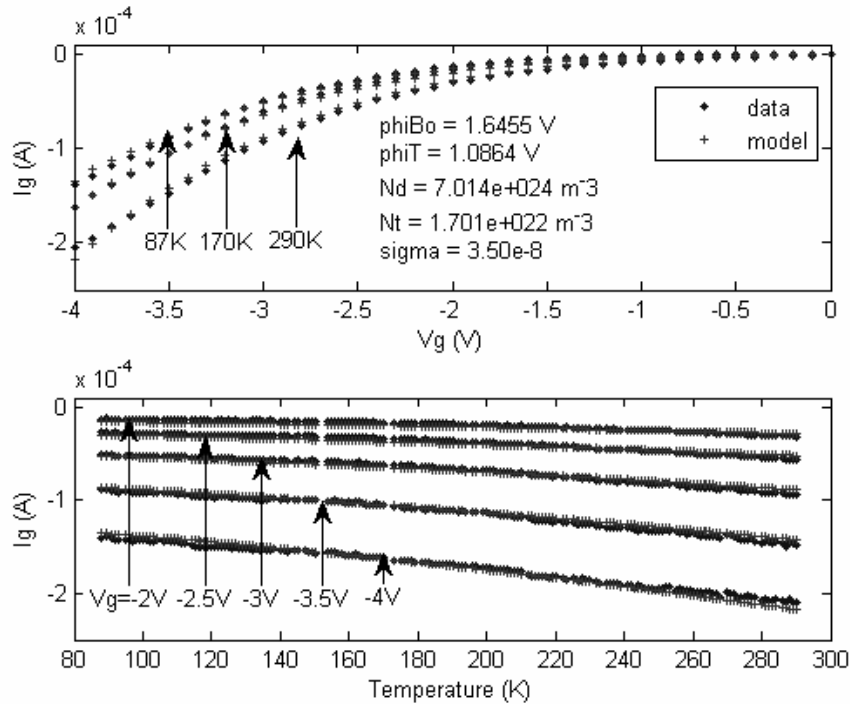and N_d (Equation 16).

Figure 39. TTT model fit to HFET A16 pre irradiation data.

Change in Vth with irradiation.

       The magnitude of the voltage at which the trap assisted tunneling behavior of the

IV curve changed to a resistive behavior appeared to increase after irradiation in all cases.

For purposes of this study this is assumed to indicate an increase in V_{th}, although that is

certainly not the only interpretation. The change in behavior for device A16 is shown in
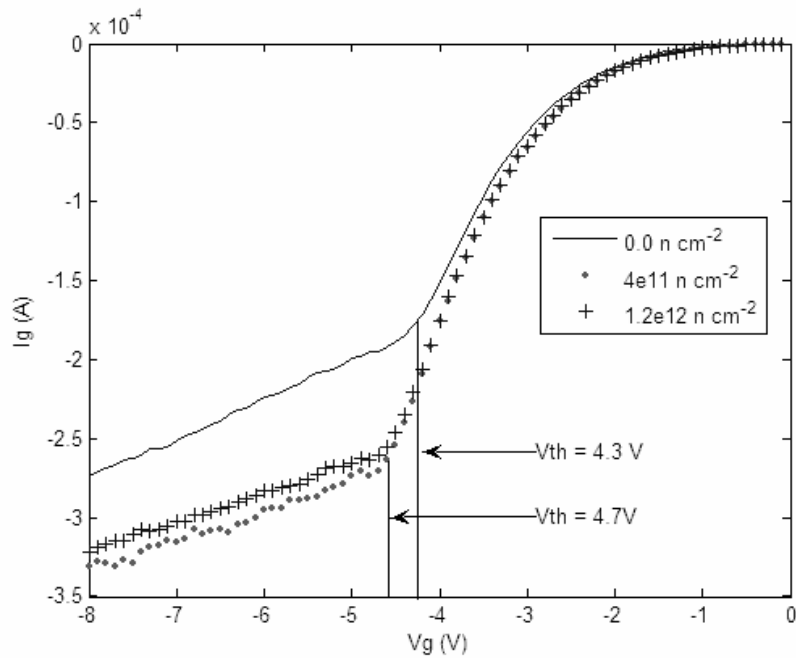
Figure 40.

Figure 40. HFET A16 0.0, 4×10^{11} and 1.2×10^{12} fluence IV curves.

Increased I_g with irradiation.

Irradiating the HFETs with high energy (>0.5 MeV) neutrons resulted in increased gate current, consistent with the effect previously reported [7,8]. The increase in I_g saturates after a fluence of approximately 10^{12} n/cm^2 with an approximately 30% increase in magnitude of current, which is also consistent with previous results [8].

HFET A16 was irradiated twice, first with a fluence of 4×10^{11} n/cm^2 and second with 1.2×10^{12} n/cm^2 (**Figure 41**). The gate current increased by approximately 30% after the first irradiation and showed less temperature dependence than the pre irradiation curve. The gate current was reduced after the second irradiation and shows a slightly greater temperature dependence than the pre irradiation curve until 260K. After 260K the current becomes constant with temperature, which may indicate an annealing process.
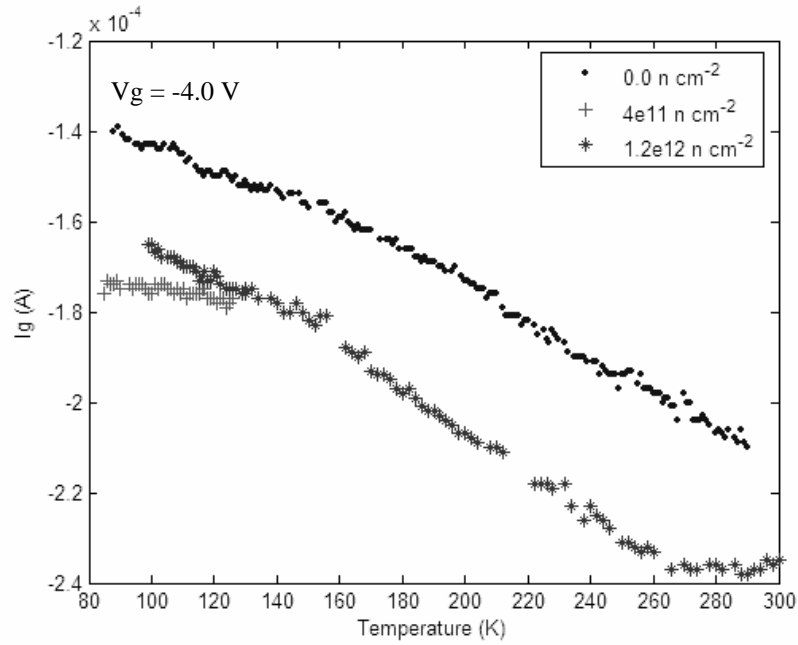
Figure 41. HFET A16 pre and post irradiation IT curves.

The TTT model was used to fit the post irradiation data in an attempt to determine whether an irradiation induced increase in N_t or decrease in ϕ_b, or combination of the two, was responsible for the increase in gate current. The TTT model was fit beginning with pre irradiation values for the primary parameters (ϕ_b, ϕ_t, N_d, N_t) and attempting to achieve the best least squares fit by varying single parameters, combinations of parameters, or constraining the values of ϕ_b and N_d using Equation 16.

The pre irradiation data was fit by constraining the values of ϕ_b and N_d using Equation 16 and using -4.3V as the value of V_{th}. This resulting in the fit presented in Figure 42. These pre-irradiation values of the primary parameters were used as a baseline in the investigation that follows.
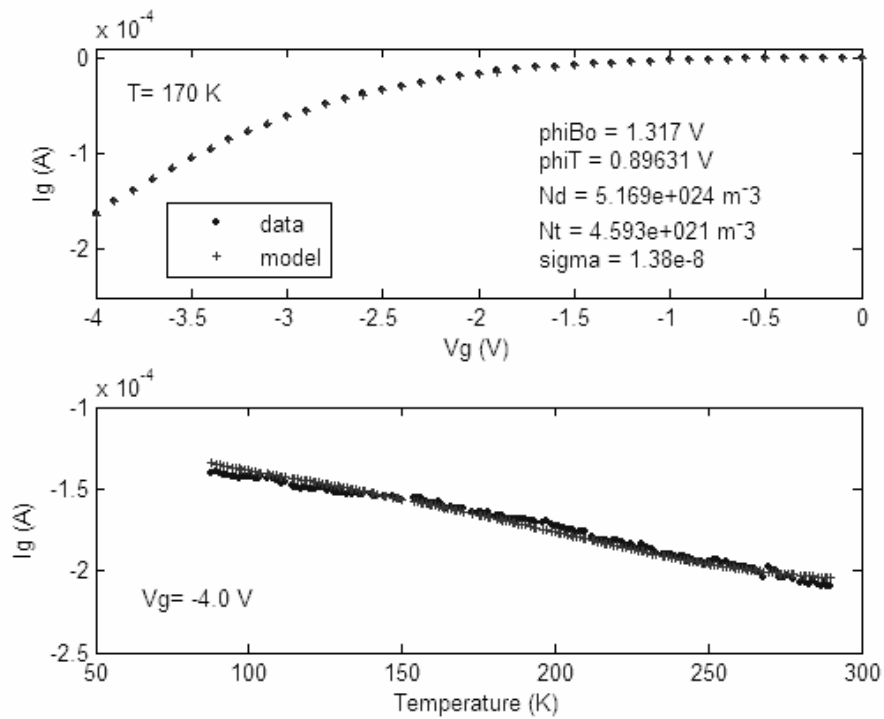
Figure 42. TTT model fit of A16 pre irradiation data with constraints.

Fitting TTT to HFET A16 4x10^{11} fluence data.

Fitting the TTT model to $4x10^{11}$ fluence data by beginning with the baseline

parameters values and allowing all parameters to vary resulted in the fit shown in Figure

43. Although this is a good fit to the data in the figure as shown by a low sigma

$(6.03x10^{-9}$ A), the fit would be very poor at higher temperatures because I_g is expected to

increase at a rate similar to the pre irradiation data while the model predicts an almost

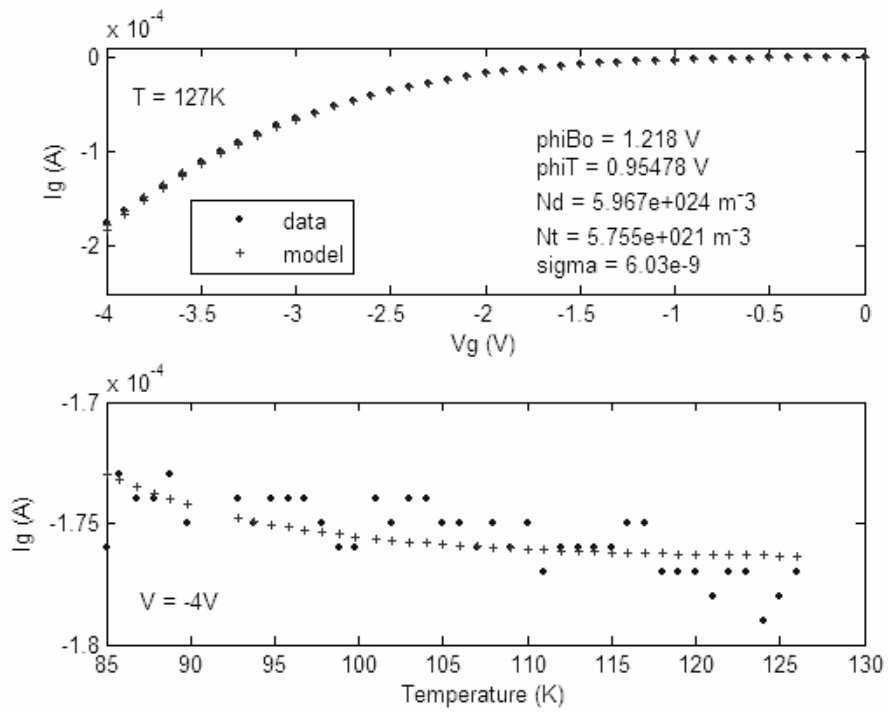constant current at temperatures above 125K.

Figure 43. TTT model fit to A16 4x10^{11} data, all parameters allowed to vary.

Varying N_t only, in an attempt to model the increase in gate current as being due to an increase in trap density only, results in the fit shown in Figure 44. The TTT model predicts a greater temperature dependence than was observed.
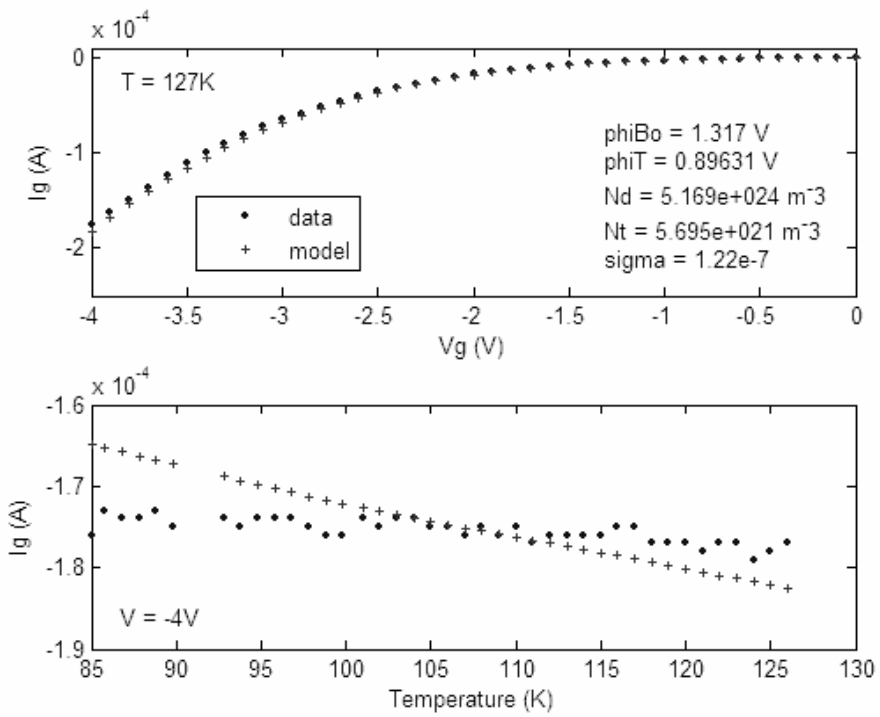
Figure 44. TTT model fit to A16 4x10^{11} data, Nt allowed to vary.

Varying ϕ_b gives the result in Figure 45. The model predicts much less temperature dependence that observed, and these parameters would result in a very poor fit at higher temperatures.
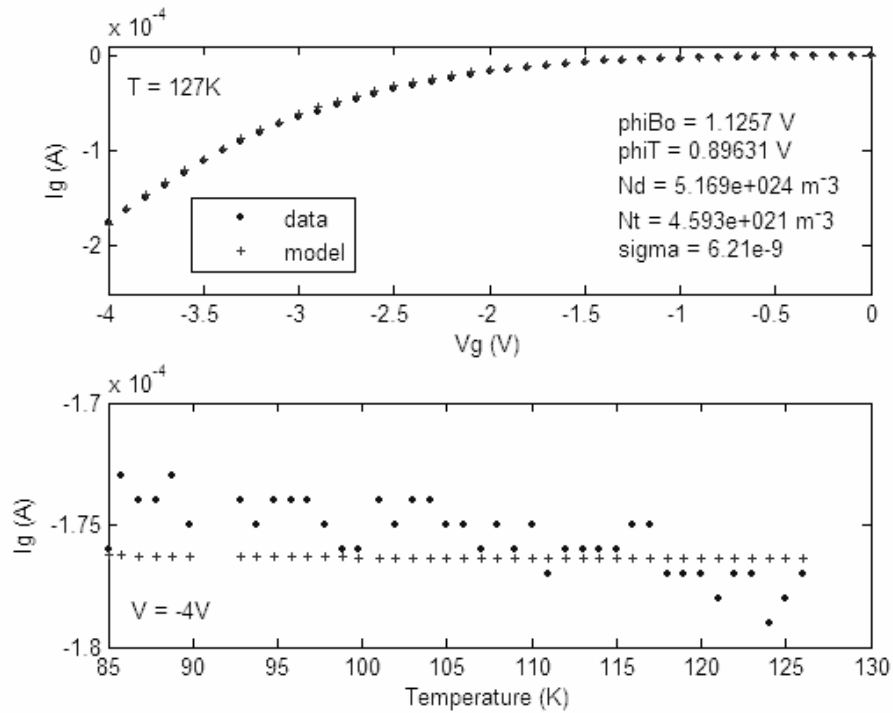
Figure 45. TTT model fit to A16 4x10^{11} data, ϕ_b allowed to vary.

It does not appear likely that trap assisted tunneling is the primary mechanism responsible for the increase in I_g after the initial, 4x10^{11} n/cm^2 irradiation of HFET A16. It seems unlikely that all four of the parameters in the TTT model changed from the pre-irradiation fitting values after the first irradiation but, as we shall see, an increase in N_t only is sufficient to explain the change after the second (1.2x10^{12}) irradiation. One explanation proposed to account for the decreased dependence on temperature after the 4x10^{11} fluence is that a resistive mechanism based on complexes was created.

Fitting TTT to HFET A16 1.2x10^{12} fluence data.

Allowing all parameters in the TTT model to vary, starting with the baseline values, resulted in a fit of 9.33x10^{-9} A shown in Figure 46. This is not a reasonable

explanation for the increase in current because it is unlikely that all of the parameters would have been changed by irradiation.
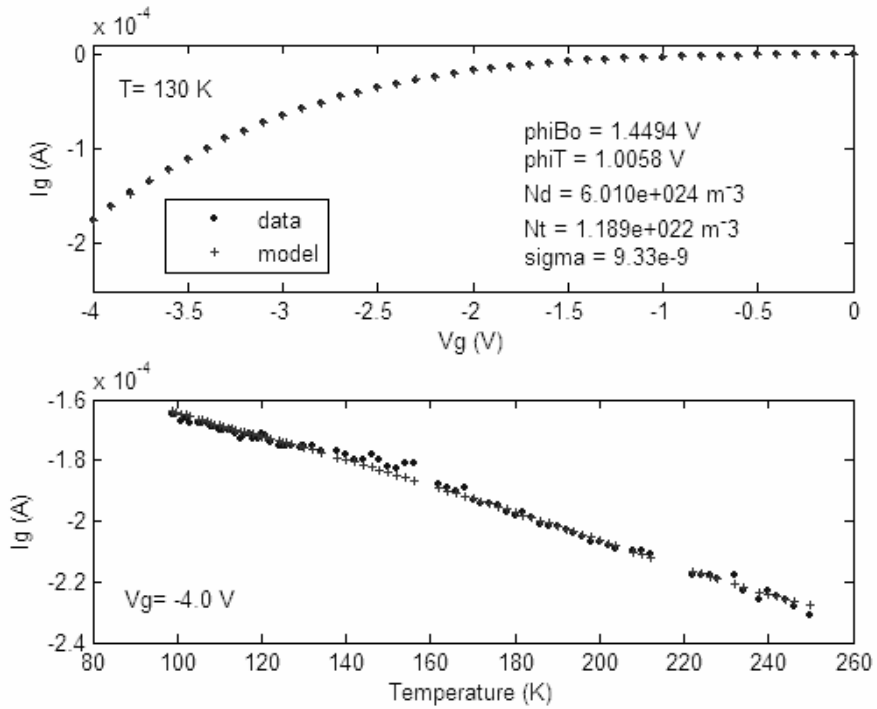

Figure 46. TTT model fit to A16 1.2x10^{12} data, all parameters allowed to vary.

Starting with baseline parameters and varying N_t only resulted in a very good fit to the data, shown in Figure 47, with a sigma of 5.63×10^{-9} A. This is a better fit than was obtained by allowing all parameters to vary in Figure 46. The fit in Figure 46 is at a 'local minima' and is consistent with how the MatLab fitting routine functions.

The improved fit in Figure 47 supports the hypothesis that the increase in current after irradiation is due to an increase in trap density. It is assumed that the traps created are at approximately the same energy as those responsible for the pre irradiation TAT current.
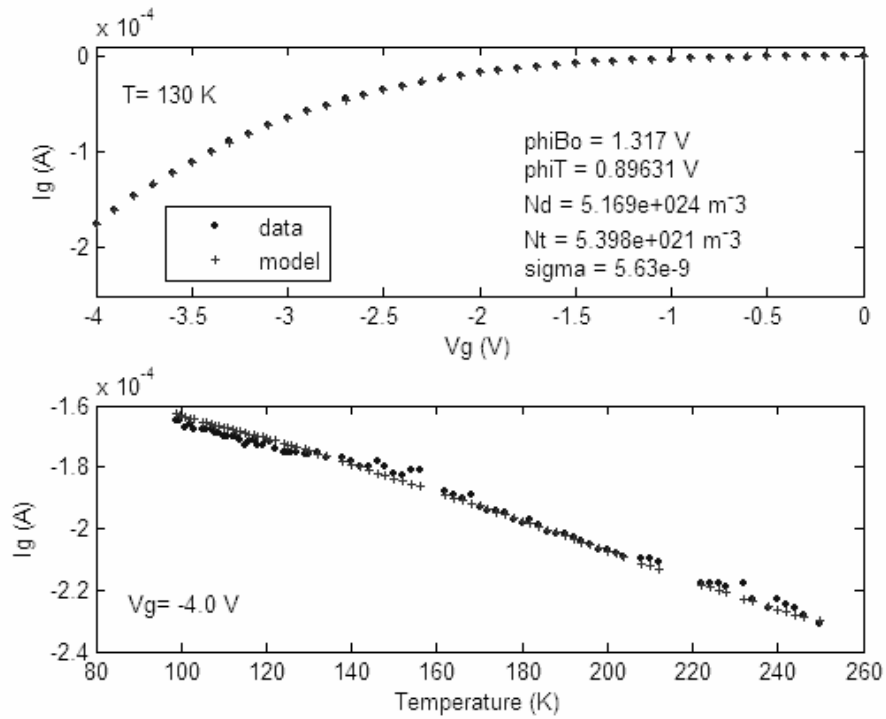
Figure 47. TTT model fit to A16 1.2x10^{12} data, N_t allowed to vary.

The traps created during irradiation would not necessarily be at the same energy as the traps responsible for the pre irradiation TAT current. To test the hypothesis that both the trap density and the trap energy changed during irradiation the model was fitted by varying N_t and ϕ_t. The result, shown in Figure 48, supports this hypothesis and suggests that both N_t and ϕ_t increased. The sigma is reduced from 5.63x10^{-9} A for varying N_t to 1.77x10^{-9} A for varying both N_t and ϕ_t. Research by Hogsed with 1MeV electrons and deep level transient spectroscopy showed that traps were created at 0.15, 0.21, 0.26 and 0.33 eV below the conduction band in AlGaN. The 0.15, 0.21 and 0.26 eV traps were found both in AlGaN and in GaN. The 0.33 eV trap was the most prominent radiation induced defect and was found only in the AlGaN. These traps are at too low an

energy to explain the increase in the effective trap energy in the TTT model (from

0.89631 pre-irradiation to 0.90282 V) after neutron irradiation. Other researchers, such

as McCluskey, et. al., have demonstrated the presence of deep traps which could explain

this proposed increase in trap energy. McClusky et. al. found a trap at 1.3 eV below the

conduction band which they contribute to an oxygen DX center [22].
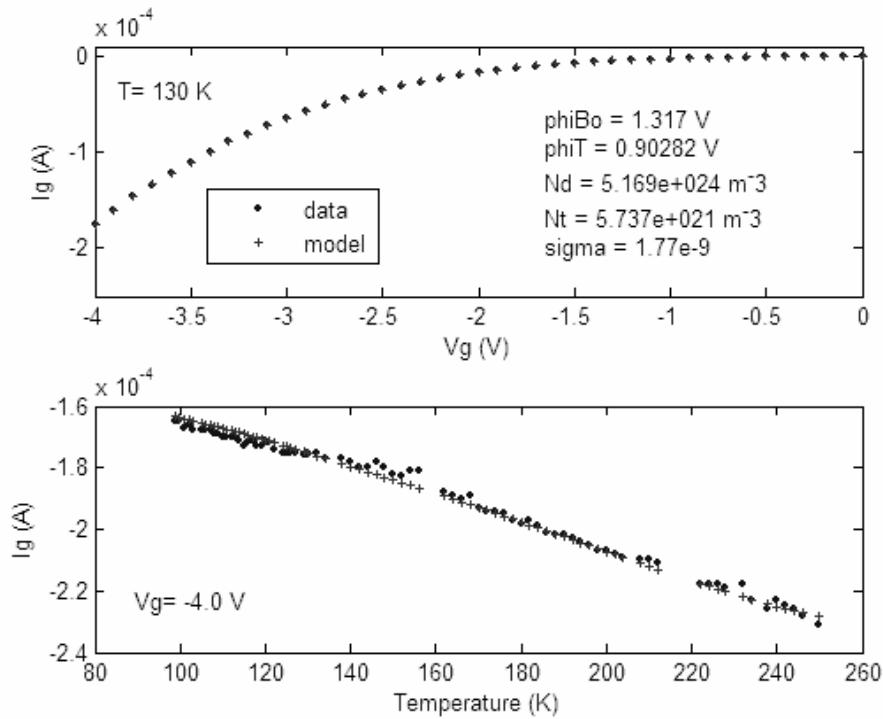
Figure 48. TTT model fit to A16 1.2x10^{12} data, N_t and ϕ_t allowed to vary.

A second hypothesis, that a change in ϕ_b and N_d is responsible for the change in

current, is tested by varying ϕ_b and N_d with $V_{th} = -4.7$V under the constraint of equation

16. This gives the result in Figure 49 with a sigma of 2.74x10^{-8} A. This fit was only

possible if ϕ_b increased, which is not consistent with the hypothesis that a decrease in

ϕ_b due to increased donor density was responsible for the increase in gate current.
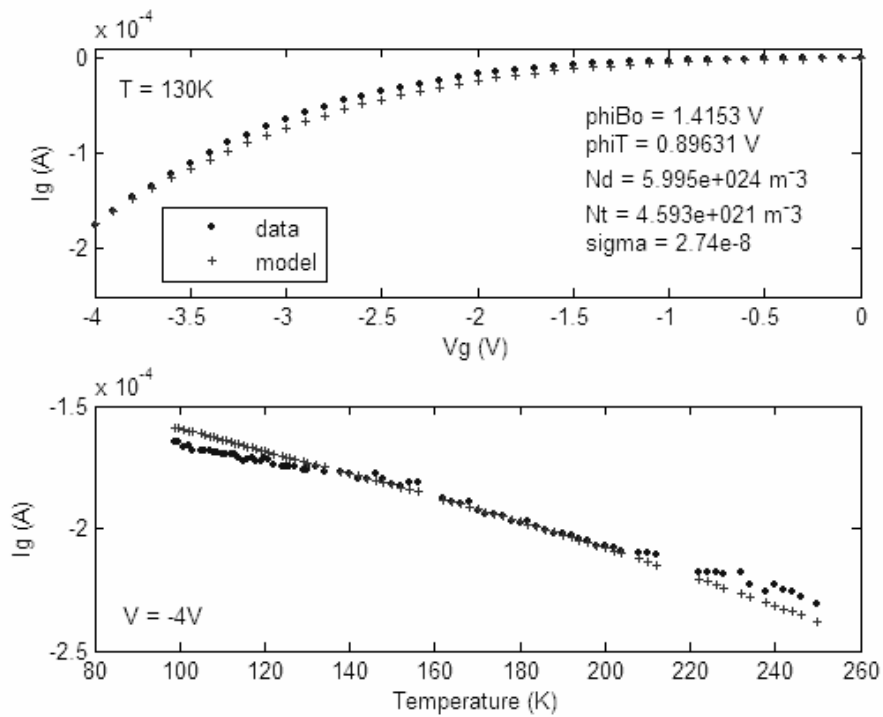
Figure 49. TTT model fit to A16 1.2×10^{12} data, ϕ_b and N_d constrained.

We could speculate that a mechanism caused a reduction in Schottky barrier height at the gate without requiring a change in N_d. Reducing ϕ_b without a change in N_d results in a poorer fit to the data (a sigma of 4.03×10^{-8} A), as shown in Figure 50. Furthermore, there is a large change in the voltage dependence at higher temperatures. This is a poor fit to the data and suggests that a change in ϕ_b only is not responsible for the increase in gate current.
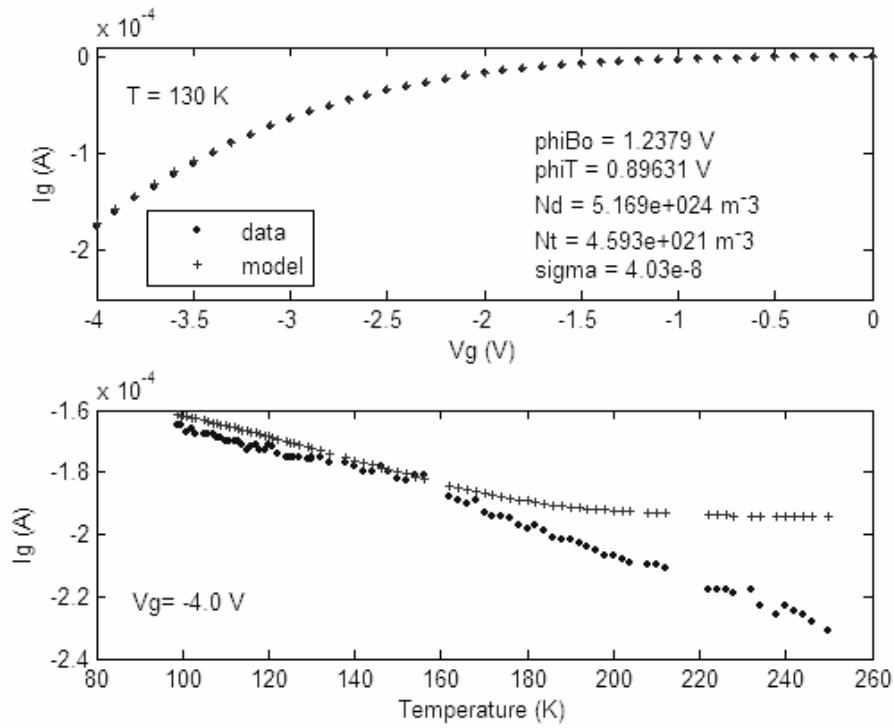
Figure 50. TTT model fit to A16 1.2x10^{12} data, ϕ_b unconstrained.

Finally, a change in N_d without a change in the other parameters is modeled to explain the increase in gate current. The fit (5.00x10^{-9} A) is better than the fit obtained by allowing only N_t to vary (5.63x10^{-9} A, Figure 47) but not as good a fit as when both N_t and ϕ_t were allowed to vary (1.77x10^{-9}, Figure 48). Using Equation 16, an increase in N_d from 5.169x10^{24} to 5.472x10^{24} donors/m^3 would increase the magnitude of V_{th} from -4.30 V to -4.48 V. This is consistent with the apparent measured increase in the magnitude of V_{th} shown in Figure 40.

Figure 51. TTT model fit to A16 1.2x10^{12} data, N_d allowed to vary.
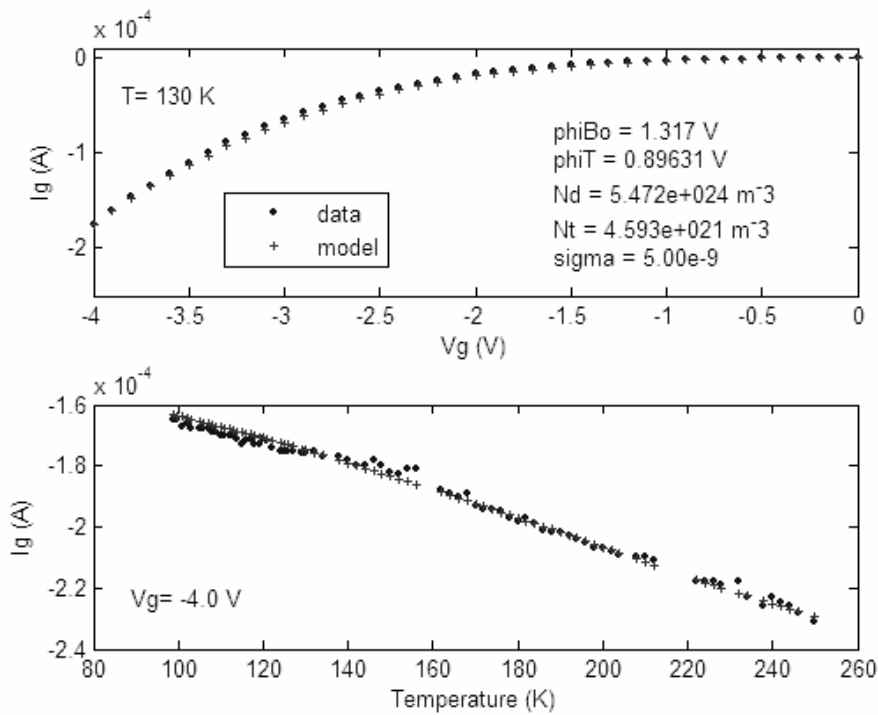
G1, G2, G3 and G4 data.

As discussed previously, HFETs G1-G4 were cut from a different section of the Cree wafer than the HFETs studied by Uhlman and Roley. Although they were mounted to the transistor package by the same lab and connected in the same way, they exhibit much more complex behavior than HFET A16 and the HFETs studied by Uhlman and Roley. While we can make qualitative comparisons among HFETs G1-G4 and between G1-G4 and A16, it is not valid to model them using the TTT model because there are clearly other mechanisms at work than trap assisted tunneling. These HFETs cannot be modeled using TTT unless these other mechanisms are identified and their contributions are eliminated.

IV and IT curves for each HFET were taken before irradiation and then at fluences of $4x10^{10}$, $8x10^{10}$, $4.8x10^{11}$ and $8.8x10^{11}$ n/cm^2. The procedure at each fluence was to measure gate current using the LabView program between approximately 85K and 120K and then measure gate current again while cooling the HFETs by 5K increments to verify the results.

HFETs G1 and G2 were mounted together on an aluminum fin, as were HFETs G3 and G4. The data for HFETs G1 and G3 was taken using SMU #16. The data for HFETs G2 and G4 was taken with SMU #17. As discussed in the procedures section, SMU#17 had a defect which was not discovered until after the experiment. The data below has been corrected except where noted.
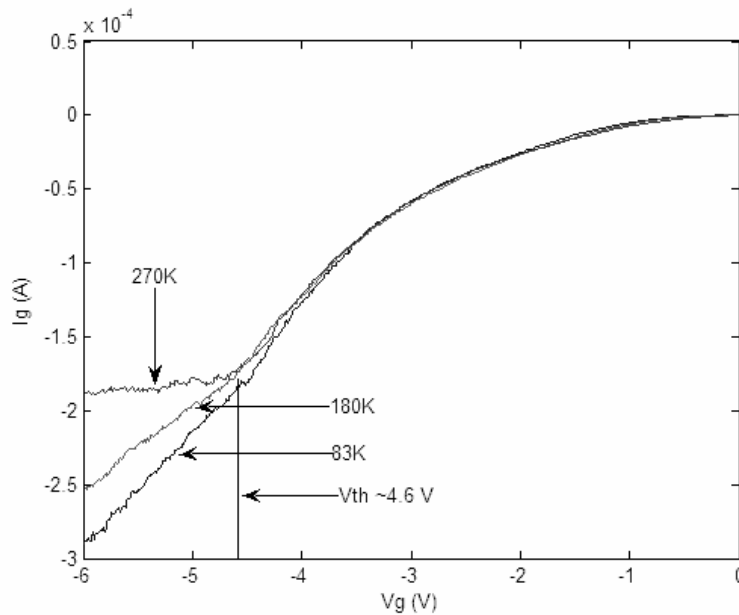
Figure 52. HFET G1 pre irradiation IV data.

The IV behavior of HFET G1 is qualitatively the same as A16, including the presence of a resistive contribution to current beyond V_{th} which becomes more resistive

(contributes less current per volt) at higher temperatures. An unexpected feature is that less, instead of more, current is observed at higher temperatures. This feature will also be observed in the IT data.

Figure 53. HFET G1 8.8x10^{11} fluence IV data.

As was the case with A16, HFET G1 shows an apparent increase in V_{th} after irradiation (Figure 53).

Figure 54. HFET G1 pre and post irradiation IT data.

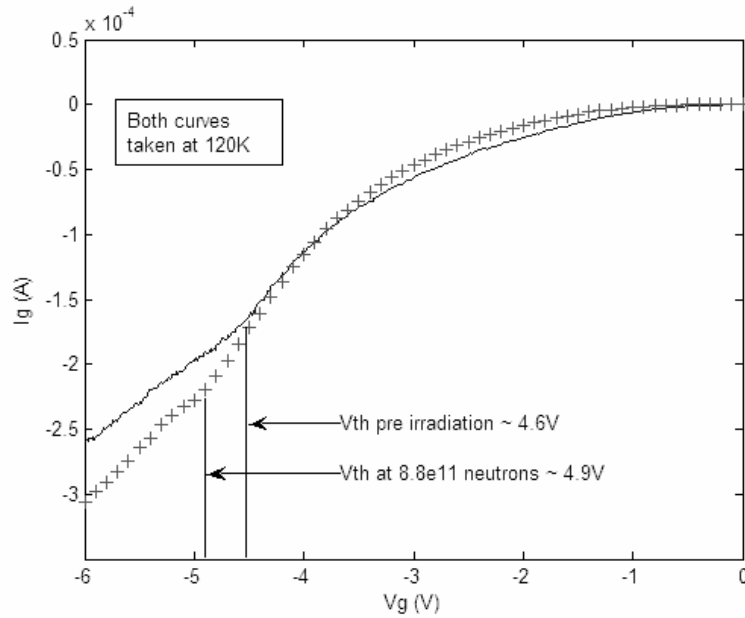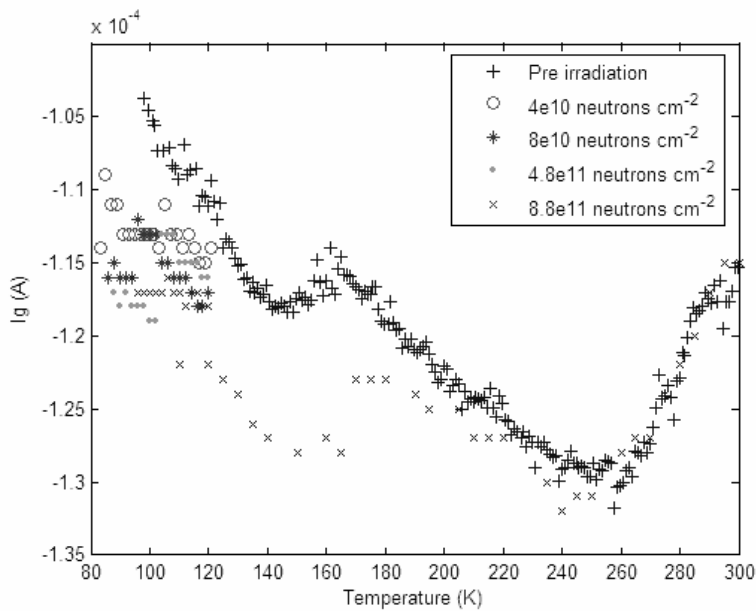The complex pre- and post-irradiation IT behavior of HFET G1 is apparent in Figure 54. The curve appears linear between 100K and 140K and between170K and 260K. The mechanism responsible for the decrease in current between 140K and 160K, and between 260K and 300K, is unknown.

After the first irradiation (4×10^{10} n/cm^2) the gate current increased nearly 10% and appears almost constant with temperature. The second irradiation (to a total of 8×10^{10} n/cm^2) increased the current to approximately 15% above the pre irradiation values between 80K and 95K. At 95K there appears to be an annealing mechanism that reduces the current. Between 95K and 120K the curve has approximately the same slope as the pre irradiation IT curve and could be explained using the TTT model. The third irradiation (to a total of 4.8×10^{11} n/cm^2) increased the current to 20% over the pre irradiation values. At 105K the current is suddenly reduced, after which it follows a

similar slope to the pre irradiation IT curve. The final irradiation (to a total of 8.8×10^{11} n/cm^2) produced an IT curve that was nearly linear with temperature between 90K and 120K. When the device had cooled to 115K another set of data was taken to 300K. The curve had the same shape as the pre irradiation curve until 170K when annealing appears to have taken place and the current showed less than a 5% increase over pre irradiation values. Beyond 250K no increase in current is observed.
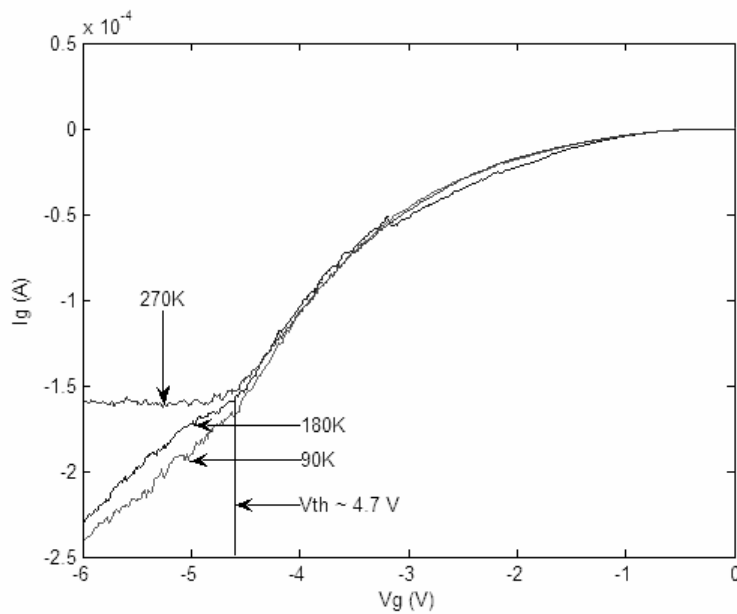
Figure 55. HFET G2 pre irradiation IV data.

The IV character of HFET G2 is qualitatively the same as for G1, including the unexpected reduction in current with temperature which will also be observed on the IT curve. The absolute magnitude of the current in Figure 55, and the shape of the curve, is not correct because of the defect in SMU #17. Therefore the data should be viewed only qualitatively.
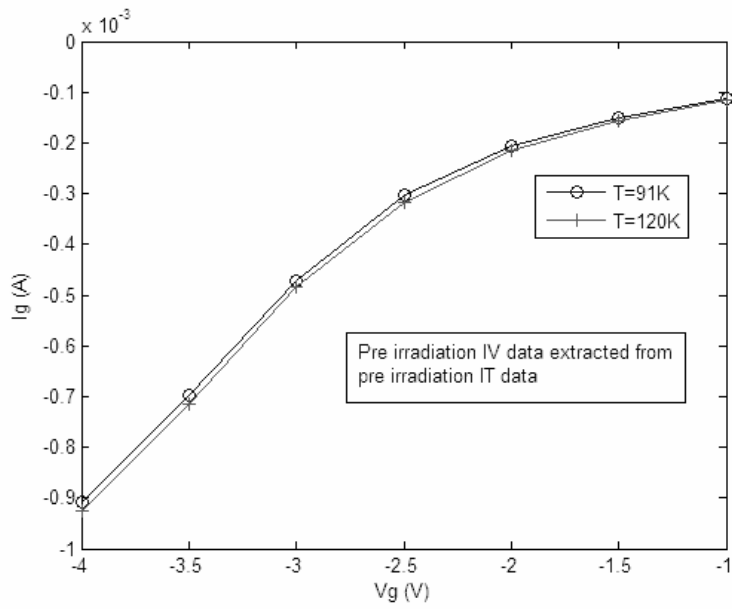
Figure 56. HFET G2 pre irradiation IV data extracted from IT data.
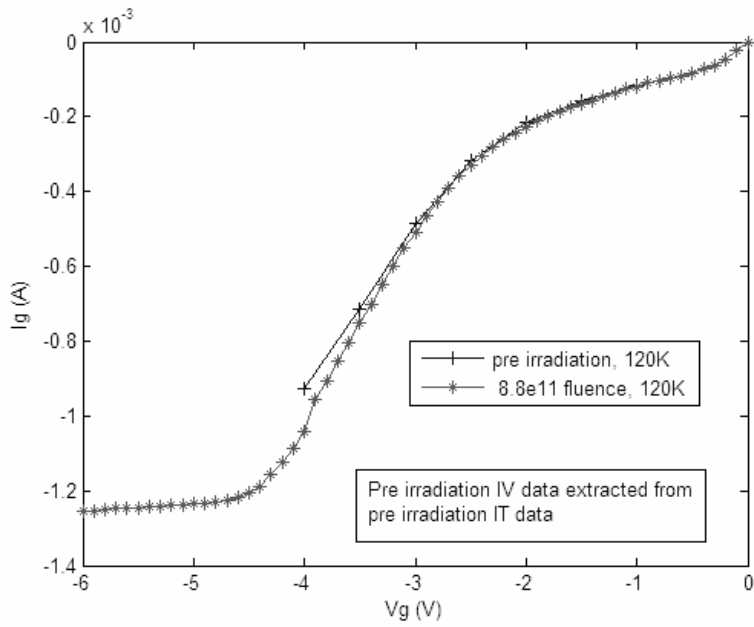
Figure 57. HFET G2 pre irradiation and 8.8x10^{11} IV data.

The change in V_{th}, if any, is indeterminate from the pre and post irradiation data. The post irradiation IV curve shows an increased current at low voltages that is greater than would be expected from trap assisted tunneling alone. This feature was not present in the pre irradiation data.
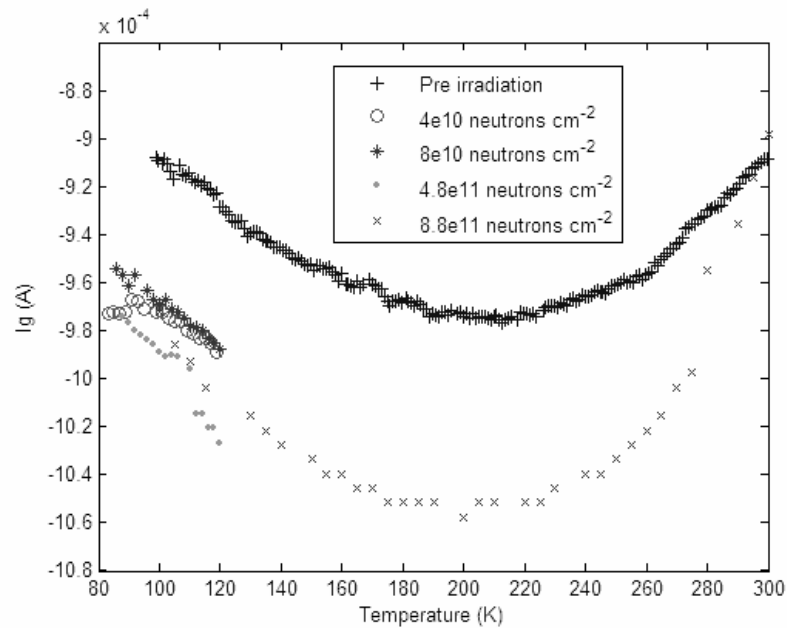
Figure 58. HFET G2 pre and post irradiation IT data.

The pre irradiation IT curve (Figure 58) is much less complex than that of HFET G1. IT appears qualitatively similar to the IT curve of A16 from 90K to 200K. Beyond 200K the current decreases in a way that is not compatible with the trap assisted tunneling model. Because of the defect in SMU #17, the voltage sourced when the measured gate current went beyond 0.1mA (at approximately 120K) was high by a factor of 1.60. This put V_g at approximately -6.4V instead of the desired -4.0V. To correct for

this the data was moved 'by eye' until it appeared to be in line with the data taken below

0.1 mA. The data below 0.1 mA was taken using the 0.1 mA circuit in SMU #17, which

was working correctly. Therefore the only conclusion that can be drawn from HFET G2

is that the magnitude of the current increased after irradiation and that the IT curve

roughly followed the shape of the pre irradiation curve.
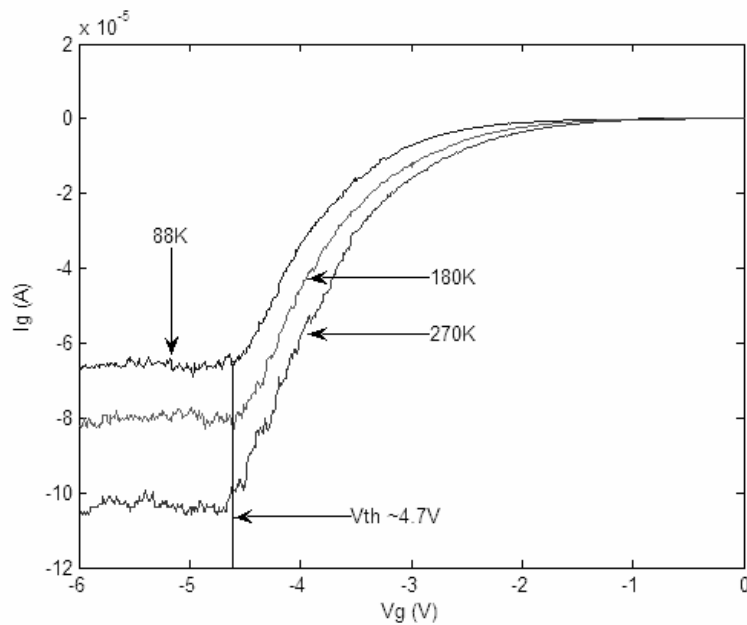
Figure 59. HFET G3 pre irradiation IV data.

HFET G3 (Figure 59) does not show the temperature dependent resistive

contribution beyond V_{th} that was observed in A16, G1 and G2. The temperature

dependence of the current is qualitatively similar to A16 with higher current at higher

temperatures.
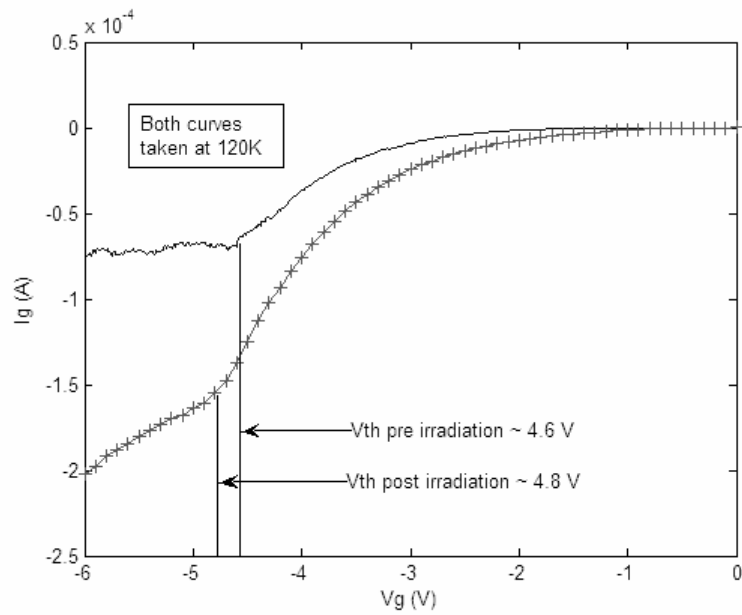
Figure 60.   HFET G3 pre irradiation and 8.8x10^{11} IV data.

The inflection in the IV curve in Figure 60, assumed to represent V_{th}, increases after irradiation as with A16 and G1. Note that a resistive mechanism beyond V_{th} has appeared after irradiation.
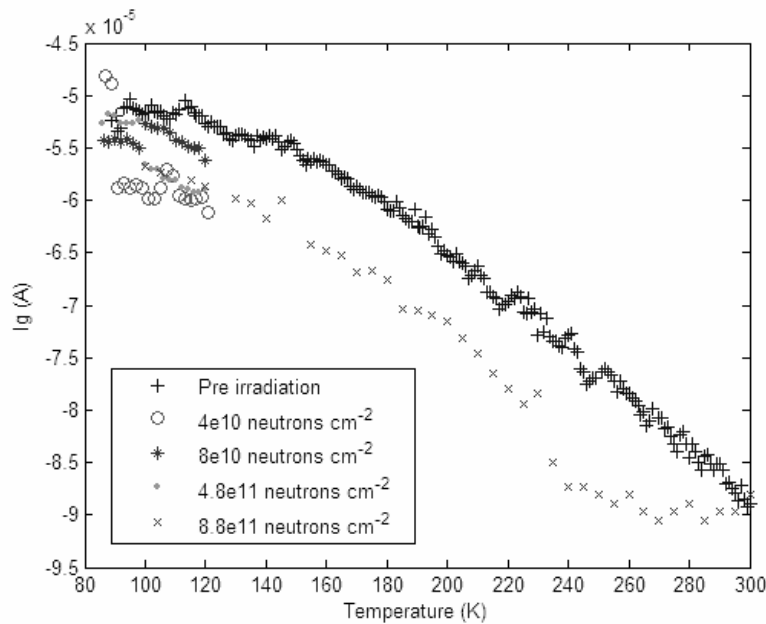
Figure 61. HFET G3 pre and post irradiation IT data.

The pre irradiation IT curve of HFET G3 is roughly linear with temperature, particularly beyond 180K (Figure 61). It also shows a much greater (factor of 6) temperature dependence than A16.

The irradiation curves show the unexpected result that the greatest increase in current occurred at the lowest fluence. The discontinuities with temperature that appeared in the HFET G1 IT curves are also evident here, with the 4×10^{10}, 8×10^{10}, and 4.8×10^{11} curves showing sudden increases or decreases with temperature. The 8.8×10^{11} post irradiation IT curve roughly parallels the pre irradiation curve until approximately 260K when the gate current returns to pre irradiation values. This is suggestive of an annealing process.
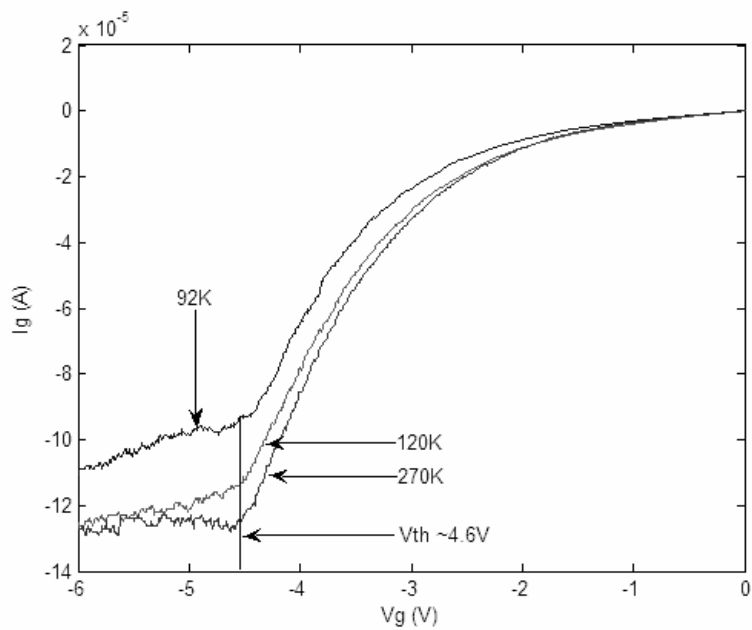
Figure 62. HFET G4 pre irradiation IV data.

The data for HFET G4 was taken with SMU #17 and should be viewed as qualitative only. From Figure 62 the gate current increases with temperature and the resistive mechanism beyond V_{th} becomes more resistive with temperature.

Figure 63. HFET G4 pre and 8.8x10^{11} IV data.
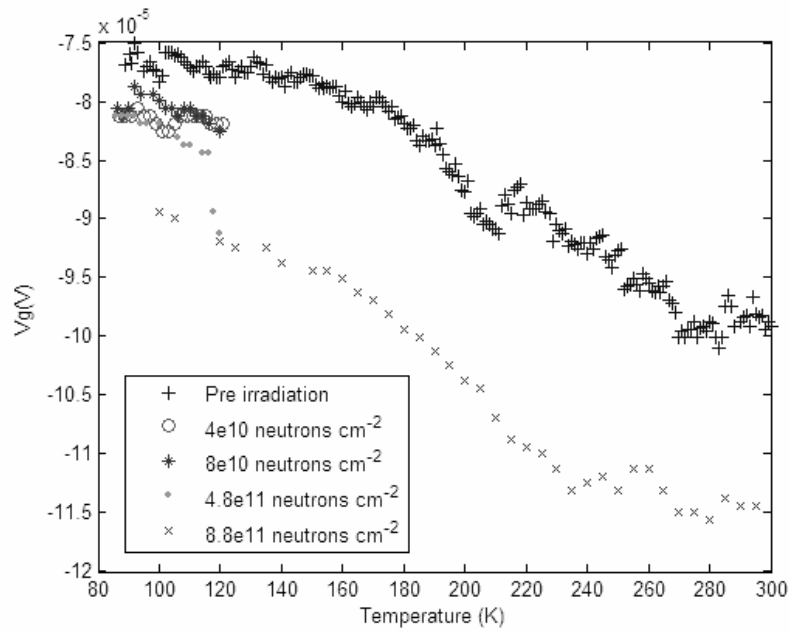
Figure 64. HFET G4 pre and post irradiation IT data.

101

The inflection of the IV curve, assumed to indicate V_{th}, increases after irradiation for HFET G4 (Figure 63).

HFET G4 shows roughly linear temperature dependence with some complex behavior around 100K, 200K and 280K (Figure 64). Both pre and post irradiation data at currents above 0.1 mA was adjusted 'by eye' to correct for the defect in SMU #17. The only conclusion that can be drawn is that the current increased with fluence and roughly paralleled the pre irradiation IT curve.
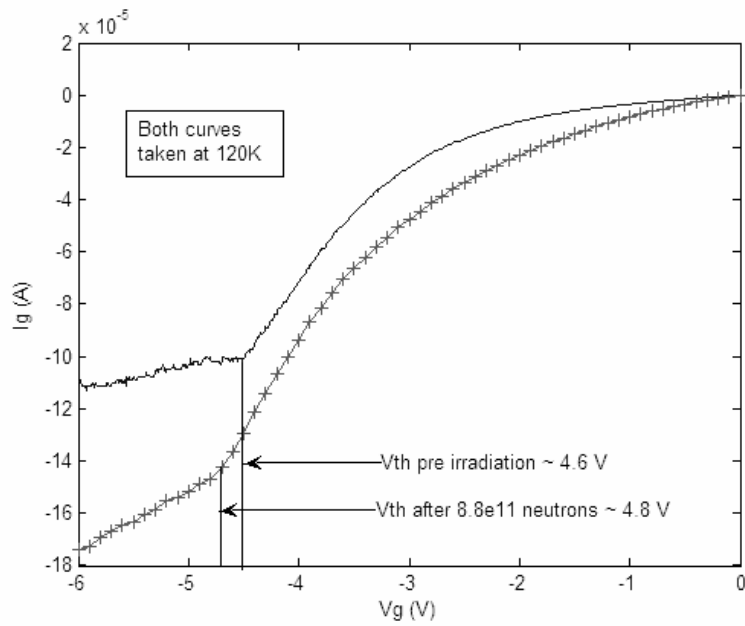
The IT curves for HFETs G1, G2 and G4 suggest a decreased dependence on temperature from 90K to 120K after the first irradiation (4×10^{10} n/cm^2) which resembles the temperature dependence observed in HFET A16 after the first irradiation (4×10^{11} n/cm^2). The IT curve HFET G3 showed little dependence on temperature both before and after the first irradiation between 90K and 120K.

Summary

HFET A16 showed gate current IV and IT behavior that was consistent with trap assisted tunneling and was fit with great success using the TTT model. The TTT model produced a least squares fit to pre-irradiation gate current within 1.38×10^{-8} A at all measured values of gate voltage and temperature using a single set of primary parameters ϕ_b, ϕ_t, N_d and N_t. The gate current was clearly not consistent with thermionic emission or thermionic field emission. Surface leakage was also eliminated as a significant contributor to because of the observation that the gate current saturated for all devices at approximately -4.5 V. An apparently resistive current mechanism produced an increase in current beyond the threshold voltage. This resistive current mechanism

showed little temperature dependence at low temperatures and rapidly became more resistive between 270K and 300K. The nature of this mechanism is unknown.

The inflection in the IV curve for A16, assumed to indicate V_{th}, shifted from -4.3 V to -4.7 volts after a fluence of 8.8×10^{11} n/cm^2. The relation between V_{th} and the gate Schottky barrier height, ϕ_b, in Equation 16 suggests that this may support the hypothesis that decreased ϕ_b is responsible for the increase in current after irradiation.

The pre and post irradiation IT curve data taken for A16 were parallel at temperatures up to approximately 260K. Above 260K the post irradiation current decreased apparently due to some annealing mechanism. This could be consistent with either the increased N_t or the decreased ϕ_b hypothesis.

The IT curve data at a fluence of 4×10^{11} n/cm^2 showed less dependence on temperature than the pre irradiation data and could not be fit by either N_t alone or ϕ_b and N_d constrained by the apparent V_{th} using equation 16. The TTT model gave a very good fit by varying all parameters. It seems highly unlikely that all parameters were changed by the irradiation, so the cause for this behavior is unknown.

The IT curve taken at 1.2×10^{12} n/cm^2 shows the same temperature dependence the pre irradiation IT curve and was fit very well (5.63×10^{-9} A) by increasing N_t and holding the other parameters fixed at the values that fit the pre irradiation data. An even better fit (1.77×10^{-9} A) was obtained by allowing N_t and ϕ_t to vary. This supports the hypothesis that an increase in trap density is responsible for the post irradiation increase in current. The data was not fit as well (2.74×10^{-8} A) when ϕ_b and N_d were varied under the

constraint of the apparent post-irradiation V_{th} (-4.7 V) using equation 14 or when ϕ_b was allowed to vary independently of the other parameters (4.03x10^{-8}). A sigma of 5.00x10^{-9} A was obtained by increasing the donor density by approximately 5.8% from 5.169x10^{24} donors/m^3 to 5.472x10^{24} donors/m^3. Equation 16 indicates that this increase in N_d would increase V_{th} from -4.3 to -4.48. This increase in the magnitude of V_{th} is consistent with the apparent increase in V_{th} observed in Figure 40. This suggests that an increase in donor defects, caused by neutron irradiation, could be responsible for both the increase in gate current and the apparent change in threshold voltage.

HFETs G1-G4 showed much more complex IT behavior than device A16, indicating that mechanisms other than trap assisted tunneling are providing a significant contribution to the gate current. This is probably due to either a defect in the section of the wafer from which G1-G4 were made or some difference in the way the devices were cut from the wafer and mounted in their housings. Furthermore, the defect in SMU #17 invalidated much of the data from HFETs G2 and G4. Therefore only qualitative conclusions can be drawn from these HFETs. G1-G4 showed increased gate current after irradiation. As with A16 the increase in current was not proportional to fluence. The gate current of HFET G1 annealed to nearly pre irradiation values at approximately 180K. The gate current of HFETs G2 and G3 annealed beginning at 260K, consistent with the results observed for A16. HFET G4 did not show any significant annealing.

The IT curves for HFETs A16, G1, G2 and G4 showed less temperature dependence between 90K and 120K after their initial irradiation. HFET G3 showed a small dependence on temperature between 90K and 120K both before and after

irradiation. The mechanism responsible for this would have to produce a current that decreased with temperature at approximately the same rate as the trap assisted tunneling mechanism current increased with temperature. The responsible mechanism is unknown.

VI. Conclusions and Recommendations

Conclusions of Research

Pre irradiation IV and IT data are consistent with the trap assisted tunneling model. The STAT and TTT models give very good fit to the measured pre irradiation gate current. It has been demonstrated that the thermionic emission, field emission, and surface leakage models do not fit the measured data. Therefore it is concluded that trap assisted tunneling is the primary mechanism responsible for gate leakage in the AlGaN/GaN HFET.

The observed increase in current and decrease in temperature dependence for HFET A16 after the first neutron irradiation (4×10^{11} n/cm^2) cannot be fit with the TTT model by varying either ϕ_b or N_t alone. Either a different mechanism is responsible for the increased gate current after that irradiation or all of the primary parameters were changed, which seems highly unlikely. The IV and IT data after the second irradiation (to a total of 1.2×10^{12} n/cm^2) was consistent with an increase in N_t. Increasing both N_t and ϕ_t resulted in the best possible fit to the data with a sigma of 1.77×10^{-9} A. Decreasing ϕ_b resulted in a very poor fit to the IT curve at higher temperatures. Varying ϕ_b and N_d under the constraint of Equation 16 resulted in a better fit, but only if ϕ_b increased and N_d decreased. Increasing ϕ_b is not consistent with the observations of White, et. al. [9,13] after proton irradiation, although a decreasing effective N_d is consistent with their observations. Finally, increasing N_d resulted in a good fit

(5.00x10^{-9} A) and, using Equation 16, resulted in an increase in magnitude of V_{th} from -

4.30 V to -4.48 V. This is consistent with the apparent increase in V_{th} observed in Figure

40. This suggests that an increase in N_d may be responsible for the increase in gate

current after irradiation.

There was not enough data generated in this research to conclude that either an

increase in density of traps or an increase in density of donor defects was responsible for

increased current after neutron irradiation. Further evidence is required which could be

obtained by using a different technique, such as Hall effect or electroluminescence.

Furthermore, the unexpected IT results for HFET A16 after a fluence of 4x10^{11} n/cm^2

need to be explained.

Recommendation for Future Research

The use of IV and IT measurement shows promise as a method to determine the

cause of increased gate current in AlGaN/GaN HFETs after irradiation. In order for this

technique to be effective the contribution of other mechanisms than trap assisted

tunneling must be eliminated. HFETs G1-G4 have large contributions to gate current

from mechanisms other than trap assisted tunneling. HFETs with more predictable

behavior, such as HFET A16, are required if this research is to continue.

The apparent reduction in magnitude of the threshold voltage with fluence should

be studied. The constraint imposed on ϕ_b and N_d by the relation in Equation 16 provides

a useful tool in the investigation.

The two mechanisms proposed for increase in gate current after irradiation, increased trap density and increased donor defect density, should be studied by irradiating HFETs and measuring trap and donor defect densities using other techniques.

The possible effect of Schottky barrier thinning due to an increase in donor defects near the AlGaN surface, as modeled by Hashizume [15] , was not explored in this research. The good fit to empirical data that Hashizume achieved warrants further research. More detail on Hashizume's method than was available in published papers must be obtained before this can be done.

Appendix

Physical Constants

Constant	Expression	Value	Units
k	Boltzmann's constant	1.38×10^{-23}	J/K
q	electronic charge	1.609×10^{-19}	Coulombs
m_e	free electron mass	9.1×10^{-31}	kg
ε_o	permittivity of free space	8.854×10^{-12}	F/m
h	Planck's constant	6.625×10^{-34}	J*s
A*	Effective Richardson's Constant	1.2×10^6	$A/m^2 K^2$

Material Parameters

Parameter	Expression	x=.27	Units	Reference
$\varepsilon(x)$	$(-0.5x + 9.5)\,8.854x10^{-12}$	$9.365\varepsilon_o$	$C\text{-}m^{-1}\text{-}V^{-1}$	[8]
$\Delta\phi_c(x)$	$(1.197x + 0.7x^2)$	0.374	eV	[8]
m_{AlGaN}	effective mass of electron in AlGaN	$.28\,m_e$	kg	[8]
$\phi_m(x)$	$(1.3x + 0.84)$	1.19	eV	[8]

HFET parameters

Parameter	Description	Value	Units
A	Gate area	5.0×10^{-9}	m^2
d	AlGaN depth	25×10^{-9}	m

Bibliography

[1]   Morkoc, H., A.D. Carlo, et al. (200) "GaN-based modulation doped FETs and UV detectors." Solid-State Electron. 46: 157-202

[2]   M. Stutzmann et al. "GaN-based heterostructures for sensor applications." Diamand Relat. Mater. 11:886-891 (2002)

[3]   Y.-F. Wu et al. "30-W/mm GaN HEMTs by Field Plate Optimization", IEEE Electron Devices Letters, Vol. 25, Nr. 3 pp. 117-9, March 2004.

[4]   Eastman, L., Mishra, U., "The Toughest Transistor Yet", pp. 28-33, IEEE Spectrum, May 2004.

[5]   Hogsed, Michael R. *Deep Level Defects in Electon-Irradiated Aluminum Gallium Nitride Grown by Molecular Beam Epitaxy.* Air Force Institute of Technology (AU), Wright-Patterson AFB OH, March 2005.

[6]   Sattler, James M. *An Analysis of the Effects of Low Energy Electron Radiation on AlxGal-xN/GaN Modulation-doped Field-effect Transistors.* Air Force Institute of Technology (AU), Wright-Patterson AFB OH, March 2004.

[7]   Roley, Daniel A. Unpublished thesis, *Trap-Assisted Tunneling in AlxGa1-xN/GaN High electron Mobility Transistors.* Air Force Institute of Technology (AU), Wright-Patterson AFB OH, March 2006.

[8]   Uhlman, Troy A. *Temperature Dependent Current-Voltage Measurements of Neutron Irradiated $Al_{0.27}Ga_{0.73}N$/GaN Modulated Doped Field Effect Transistors.* Air Force Institute of Technology (AU), Wright-Patterson AFB OH, March 2005.

[9]   White, B.D. et. al. "Characterization of 1.8-MeV Proton-Irradiated AlGaN/GaN Field-Effect Transistor Structures by Nanoscale Depth-Resolved Luminescence Spectroscopy." IEEE Transactions on Nuclear Science, 49(6):2695-2701 (2002)

[10]   Sze., S.M. (1981). Physics of Semiconductor devices. New York, Wiley.

[11]   Yang, E.S. (1988). Microelectronic Devices. New York. McGraw-Hill.

[12]   Svensson, C. and I. Lundstrom. "Trap-assisted charge injection in NMOS structures." Journal of Applied Physics, 44(10): 4657-4662 (1973).

[13]   White, B.D. et. al. Proceedings of the 2004 Multi-University Research Intiative (MURI) Radiation Physics annual review sponsored by AFOSR/NE under MURI grant F49620-99-1-0289.

[14]   Hu, X. et. al. "Proton-Irradiation Effects on AlGaN/AlN/GaN High Electron Mobility Transistors." IEEE Transaction on Nuclear Science, 50(6):1791-1796 (2003).

[15]   Karmalkar, S. et. al. "Mechanism of the reverse gate leakage in AlGaN/GaN high electron mobility transistors," Applied Physics Letters, 82(22): 3976-3978 (2003).

[16]   Sathaiya, D. et. al. "Thermionic trap-assisted tunelljng model and its application to leakage current in nitrided oxides and AlGaN/GaN high electron mobility transistors." Journal of Applied Physics, 99, 093701 (2006).

[17]   Hashizume, T. et. al. "Leakage Mechanism in GaN and AlGaN Schottky interfaces." Applied Physics Letters, 84(24):4884-4887 (2004).

[18]   Answar, E.W. et. al. " Schottky barrier height in GaN/AlGaN heterostructures." Solid-State Electronics, 50:1041-1045 (2006).

[19]   Petrosky, J. "Characterization of HgCdTe Diodes Using Pisces-IIB and Implications to Radiation Effects." Rensselaer Polytechnic Institute, Troy New York, April 1992.

[20]   Greene, Kevin D. "Electron Paramagnetic Resonance Spectroscopy and Hall Effect Studies of the Effects of Low Energy Electron Irradiation on Gallium Nitride." Air Force Institute of Technology (AU), Wright-Patterson AFB OH, September 2003 AFIT/DSP/ENP/03-02.

[21]   Ionascut-Nedecescu, A. et. al. "Radiation Hardness of Gallium Nitride." IEEE Transactions on Nuclear Science, 39(6):2733-2738 (2002).

[22]   McCluskey, M. et. al. "Evidence for Oxygen DX Centers in AlGaN" Mat. Res. Soc. Symp. Proc., 512:531-6 (1998).

REPORT DOCUMENTATION PAGE

Form Approved
OMB No. 074-0188

1. REPORT DATE *(DD-MM-YYYY)*	2. REPORT TYPE	3. DATES COVERED *(From – To)*
07-03-2007	Master's Thesis	October 2007 – March 2007

4. TITLE AND SUBTITLE

INVESTIGATION OF GATE CURRENT IN NEUTRON IRRADIATED $Al_XGa_{1-x}N$/GaN HETEROGENEOUS FIELD EFFECT TRANSISTORS USING VOLTAGE AND TEMPERATURE DEPENDENCE

5a. CONTRACT NUMBER

5b. GRANT NUMBER

5c. PROGRAM ELEMENT NUMBER

6. AUTHOR(S)

Gray, Thomas E., MAJ, USA

5d. PROJECT NUMBER

5e. TASK NUMBER

5f. WORK UNIT NUMBER

7. PERFORMING ORGANIZATION NAMES(S) AND ADDRESS(S)

Air Force Institute of Technology
Graduate School of Engineering and Management (AFIT/EN)
2950 Hobson Way, Building 640
WPAFB OH 45433-8865

8. PERFORMING ORGANIZATION REPORT NUMBER

AFIT/GNE/ENP/07-02

9. SPONSORING/MONITORING AGENCY NAME(S) AND ADDRESS(ES)

10. SPONSOR/MONITOR'S ACRONYM(S)

11. SPONSOR/MONITOR'S REPORT NUMBER(S)

12. DISTRIBUTION/AVAILABILITY STATEMENT

APPROVED FOR PUBLIC RELEASE; DISTRIBUTION UNLIMITED.

13. SUPPLEMENTARY NOTES

14. ABSTRACT

The gate current of $Al_{27}Ga_{73}N$/GaN heterogeneous field effect transistors (HFETs) is investigated using current-voltage (IV) and current-temperature (IT) measurement demonstrating that trap assisted tunneling (TAT) is the primary current mechanism. A thermionic trap assisted tunneling (TTT) model is used with variables of Schottky barrier height, trap energy, donor density and trap density. This results in a sigma of 1.38×10^{-8} A for IT data measured between 85K and 290K and for IV data measured between 0.0 V and -4.0 V.

High energy (>0.5 MeV) neutron irradiation confirms an increase of gate current with fluence. An increase in magnitude of threshold voltage is also observed. The TTT model suggests that increased trap density is responsible for increased gate current at a fluence of 1.2×10^{12}. An increase in trap density from the unirradiated fit value of 4.593×10^{21} to 5.737×10^{21} traps/m^3 and an increase in the position of traps in the energy band from 0.896 to 0.9028 V results in a fit with σ of 1.77×10^{-9} A. An increase in donor defect density is modeled resulting in a sigma of 5.00×10^{-9} A and an increase in threshold voltage magnitude consistent with the observed change in measured IV behavior.

15. SUBJECT TERMS

Aluminum Gallium Nitride, Gallium Nitride, Current-Voltage, Temperature-dependent Current-Voltage, HFET, AlGaN, GaN, AlGaN/GaN, I-V, I-V-T, neutron, radiation, trap-assisted tunneling

16. SECURITY CLASSIFICATION OF:			17. LIMITATION OF ABSTRACT	18. NUMBER OF PAGES	19a. NAME OF RESPONSIBLE PERSON
a. REPORT	**b. ABSTRACT**	**c. THIS PAGE**			Dr. James C. Petrosky, (ENP)
U	U	U	UU	125	**19b. TELEPHONE NUMBER** *(Include area code)* (937) 255-3636, ext 4562 (James.Petrosky@afit.edu)

Standard Form 298 (Rev. 8-98)
Prescribed by ANSI Std. Z39-18